Nanoscale Horizons

MINIREVIEW

View Article Online
View Journal | View Issue

Check for updates

Cite this: *Nanoscale Horiz.*, 2019, **4**, 117

Graphene oxide and carbon dots as broad-spectrum antimicrobial agents – a minireview

Anisha Anand,[a] Binesh Unnikrishnan,[a] Shih-Chun Wei,[b] C. Perry Chou,*[c] Li-Zhi Zhang[d] and Chih-Ching Huang*[aef]

Due to the increasing global population, growing contamination of water and air, and wide spread of infectious diseases, antibiotics are extensively used as a major antibacterial drug. However, many microbes have developed resistance to antibiotics through mutation over time. As an alternative to antibiotics, antimicrobial nanomaterials have attracted great attention due to their advantageous properties and unique mechanisms of action toward microbes. They inhibit bacterial growth and destroy cells through complex mechanisms, making it difficult for bacteria to develop drug resistance, though some health concerns related to biocompatibility remain for practical applications. Among various antibacterial nanomaterials, carbon-based materials, especially graphene oxide (GO) and carbon dots (C-Dots), are promising candidates due to the ease of production and functionalization, high dispersibility in aqueous media, and promising biocompatibility. The antibacterial properties of these nanomaterials can be easily adjusted by surface modification. They are promising materials for future applications against multidrug-resistant bacteria based on their strong capacity in disruption of microbial membranes. Though many studies have reported excellent antibacterial activity of carbon nanomaterials, their impact on the environment and living organisms is of concern due to the accumulatory and cytotoxic effects. In this review, we discuss antimicrobial applications of the functional carbon nanomaterials (GO and C-Dots), their antibacterial mechanisms, factors affecting antibacterial activity, and concerns regarding cytotoxicity.

Received 10th July 2018,
Accepted 5th September 2018

DOI: 10.1039/c8nh00174j

rsc.li/nanoscale-horizons

Published on 05 Waysu 2018. Downloaded on 01/08/2024 7:53:25 AM.

[a] *Department of Bioscience and Biotechnology, National Taiwan Ocean University, Keelung 20224, Taiwan. E-mail: huanging@ntou.edu.tw*
[b] *Department of Chemistry, National Taiwan University, Taipei 10617, Taiwan*
[c] *Department of Chemical Engineering, University of Waterloo, Waterloo N2L 3G1, Ontario, Canada. E-mail: cpchou@uwaterloo.ca*
[d] *Key Laboratory of Enhanced Heat Transfer and Energy Conservation of Education Ministry, School of Chemistry and Chemical Engineering, South China University of Technology, Guangzhou 510640, China*
[e] *Center of Excellence for the Oceans, National Taiwan Ocean University, Keelung 20224, Taiwan*
[f] *School of Pharmacy, College of Pharmacy, Kaohsiung Medical University, Kaohsiung 80708, Taiwan*

Anisha Anand

Anisha Anand is currently working as a Postdoctoral Fellow in the Department of Bioscience and Biotechnology, National Taiwan Ocean University, Keelung, Taiwan. She received her PhD degree (2013) from Avinashilingam University, Coimbatore, India. Her research interests include the synthesis and characterization of nanomaterials, nanofiltration, and sea water desalination.

Binesh Unnikrishnan

Binesh Unnikrishnan is currently working as a Postdoctoral Fellow in the Department of Bioscience and Biotechnology, National Taiwan Ocean University, Keelung, Taiwan. He received his PhD degree (2012) from National Taipei University of Technology, Taipei, Taiwan. His research interests include synthesis of functional nanomaterials and quantum dots and their applications as biosensors, electrocatalysts, supercapacitors, nanomedicine and nanozymes.

Published on 05 Waysu 2018. Downloaded on 01/08/2024 7:53:25 AM.

1. Introduction

The continual increase in human population has contributed to the pollution and contamination of air and water, which in turn has resulted in a wide spread of pathogens and infectious diseases. Due to the extensive use of antibiotics, such as fluoroquinolones, chloramphenicol, trimethoprim and various carbapenem and β-lactam antibiotics, over the past decades, many pathogens have become drug-resistant. The simultaneous use of different antibiotics has exacerbated the antibiotic resistance.[1] The resistance mechanism can vary from species to species.[2] For example, Gram-negative bacteria, such as *Escherichia coli* (*E. coli*), restrict the entry of antibiotics into the cell with the outer membrane,[3] and they can change the nature of the cell wall, making them unrecognizable to the antibiotic.[2,4] Gram-positive bacteria, such as *Klebsiella pneumoniae* (*K. pneumoniae*) and *Staphylococcus aureus* (*S. aureus*), express enzymes that are capable of modifying or destroying the drug molecule.[4] These drug-resistant superbugs cause sepsis, which increases the mortality rate.

The development of new antimicrobial agents with superior properties and specificity is critical in this era of ever-increasing drug resistance. Most new antibiotic drugs are derived by structural or functional modification of existing antibiotics.[5,6] However, developing drug-resistance against the antibiotic derivatives is also fast. While several alternative chemicals, such as peptidomimetic antimicrobials, aminoglycosides and derivatives, and FimH inhibitors, have been developed accordingly,[7–10] studies have also revealed that bacteria can develop resistance to these compounds.[11,12] On the other hand, a large variety of

Shih-Chun Wei

Shih-Chun Wei is a PhD student in the Department of Chemistry, National Taiwan University, Taiwan, conducting his research work under the supervision of Dr. Huan-Tsung Chang. He received his BSc and MSc degrees from the Department of Bioscience and Biotechnology (2007–2013), National Taiwan Ocean University, Keelung, Taiwan. His research interest is synthesis of functional nanocomposites for biosensor and nanodrug applications.

C. Perry Chou

C. Perry Chou is a Professor in Chemical Engineering with a cross appointment in Biology at the University of Waterloo, Waterloo, Canada. He received his BSc (1984) and MSc (1987) degrees from National Taiwan University, Taipei, Taiwan and PhD degree (1995) from Rice University, Houston, USA, all in Chemical Engineering. He has been involved in developing integrated biochemical, genetic, and metabolic engineering strategies to enhance biomanufacturing with various microorganisms as cell factories. He has been serving as a journal editor for Biotechnology Advances (Elsevier) since 2005.

Li-Zhi Zhang

Li-Zhi Zhang is a Professor at South China University of Technology, Guangzhou, China. He received his PhD degree (1998) from Dalian University of Technology, Dalian, China. He then conducted his postdoctoral research at Tsinghua University, Beijing, China during 1998–2000, and at Hong Kong Polytechnic University during 2000–2003. In 2003, he joined South China University of Technology. He has been involved in energy recovery, heat and mass transfer, and advanced humidity control technologies since 1992. He is currently on the editorial board of international journals, including Energy and Buildings, Indoor and Built Environment, and Thermal Science. He was awarded by the National Science Fund as a Distinguished Young Scholar of China (2014).

Chih-Ching Huang

Chih-Ching Huang is a Professor in the Department of Bioscience and Biotechnology, National Taiwan Ocean University, Keelung, Taiwan. He received his PhD degree (2004) in Analytical Chemistry from the Department of Chemistry, National Taiwan University, Taipei, Taiwan. He then worked as a Postdoctoral fellow at the same institute during 2006–2008. In 2008, he joined the Department of Bioscience and Biotechnology, National Taiwan Ocean University, Keelung, Taiwan. His research work is mainly focused on the development of nanosensors and nanodrugs. Currently, he is a Visiting Professor at the University of Waterloo, Waterloo, Canada.

 This journal is © The Royal Society of Chemistry 2019

Published on 05 Waysu 2018. Downloaded on 01/08/2024 7:53:25 AM.

nanomaterials with specific intrinsic biological properties have been developed as nanomedicine.[13,14] Several nanomaterials are known to exhibit antibacterial properties. In particular, metal and metal oxide nanoparticles have been widely studied for their potential use as a biocide.[15,16] Though these metal (*e.g.*, Ag and Au) and metal oxide (*e.g.*, CuO, Fe_2O_3, and ZnO) nanoparticles possess antibacterial activity, the release of metal ions has generated the need to replace them with safer nanomaterials.[17–19] Recently, less toxic carbon-based nanomaterials have been identified as potential antimicrobial agents. Carbon materials are environmentally friendly and used in daily life with minimal cytotoxicity. Graphene-based nanomaterials and carbon dots (C-Dots) are widely employed in medicine and life sciences research, such as drug delivery, bioimaging, photothermal therapy, gene delivery and cell-based tissue engineering.[20–25] Graphene is a thin material with a single-atom thickness and sp^2-bonded carbon atoms densely packed in a honeycomb crystal lattice. The high hydrophobicity of graphene makes it insoluble in aqueous medium and, thus, rarely employed for biological applications.[22] However, graphene oxide (GO) has both sp^2 carbons and oxygen-containing functional groups, making it amphiphilic. Because of the hydrophilicity and high dispersion of GO in aqueous medium, ease of synthesis, tunable size, low cytotoxicity, and high biocompatibility, GO serves as an important material for biological applications, including its use as an antimicrobial agent.[22,26] The presence of functional groups, such as hydroxyl, carboxyl, epoxy, *etc.*, facilitates the functionalization of GO for its interaction with biomolecules, such as proteins and nucleic acids. Szunerits and Boukherroub have provided a detailed review on the antibacterial effect of pristine graphene, GO, reduced graphene oxide (rGO) and graphene-based composites with polymers, metals and metal oxides.[27] A review on the current status of the application of graphene materials in antimicrobial nanomedicine has been published.[28] On the other hand, with sizes below 10 nm, C-Dots are composed of hybridized sp^2 and sp^3 core carbon atoms with various functional groups forming a shell structure though its exact structure is not completely revealed.[21] C-Dots can be synthesized from several precursors, such as citric acid, ammonium citrate, polyamines, and sugars.[21] Because of their extremely small size, tunable functional properties, high surface charge, and a variety of synthetic methods and precursors, C-Dots are promising and popular for many biological and biotechnological applications.[29] A key advantage for C-Dots is that the functional properties and charge of the surface can be easily manipulated during the synthesis or post-modification stage, which is highly useful in biolabeling and specific targeting of analytes or cells[21,24,30,31] as well as antibacterial applications.[32] Recently, novel C-Dots synthesized from spermine were reported to interact with the cell membrane of *E. coli* for cell disruption.[32] Such interaction induces the formation of reactive oxygen species (ROS), increasing the oxidative stress and causing the fragmentation of genomic DNA and loss of cellular structural integrity.[32]

In general, the high surface area for multivalent interaction with microorganisms makes nanomaterials more effective than conventional antibiotics.[33] The level of the interaction depends on the composition, size, shape, and surface properties of the nanomaterials, as well as the nature of the microorganism.[24,34,35] Most antibacterial studies use *E. coli*, a Gram-negative bacterium often associated with food poisoning, diarrhea and urinary tract disorders, as the model organism. Besides *E. coli*, the antibacterial efficiency of carbon-based nanomaterials has been widely studied in other common human pathogens, including *S. aureus*, *Listeria monocytogenes* (*L. monocytogenes*), *Streptococcus mutans* (*S. mutans*) and *Pseudomonas aeruginosa* (*P. aeruginosa*).[24,36] Considering the seriousness of antibiotic resistance, the World Health Organization (WHO) has published a priority list of antibiotic-resistant bacteria.[1] As a result, developing new antibacterial agents for combating a variety of antibiotic-resistant bacteria has recently gained significant attention.[5] While many reviews have been published to describe the properties, applications and functional mechanisms of various antibacterial nanoparticles,[37–41] the easily prepared and highly diverse carbon-based nanomaterials, in particular GO and C-Dots, are rarely discussed. Note that the antibacterial properties of GO and C-Dots are rather comparable with several important metal and metal oxide materials (Table 1). In addition to antibacterial activity, graphene derivatives and C-Dots exhibit potential antiviral properties, which are dependent on their surface charge, concentration, and incubation time.[42–44] However, in this review, we confine our discussion to antibacterial activities only.

In light of the extensive application of GO and C-Dots in medicine, food, cosmetics, and water treatment, the cytotoxicity and biocompatibility of the nanomaterial-based formulation can be critical. Recently, Resende *et al.* reviewed antimicrobial activity, cytotoxicity and biocompatibility of graphene-based nanomaterials, both *in vitro* and *in vivo*, for various microorganisms, mammalian cells, plants, and animals.[45] The cytotoxicity of graphene-based materials is related with various nanomaterial properties, such as the size, shape, morphology, dispersibility, functional groups, dosage, and exposure time.[45,46] However, the inconsistent antibacterial ability of GO when being applied *in vitro* and *in vivo* has compromised the potential of GO as an antibacterial agent.[47] Several factors might contribute to this phenomenon, in particular, the undesired adsorption of biomolecules on the GO surface and the size, morphology, and purity of GO. In contrast, C-Dots, which are much smaller than GO, have shown promising and consistent antibacterial activity, both *in vitro* and *in vivo*.[24] In-depth understanding of various nanomaterial properties and their influence on the antibacterial mechanism and cytotoxicity is critical for developing effective carbon-based antibacterial agents. By focusing on GO and C-Dots, this review summarizes their antibacterial mechanisms, factors influencing their antibacterial efficacy, their practical applications and the associated biocompatibility and cytotoxicity.

2. GO as an antimicrobial agent

The interaction between graphene-based nanomaterials and microorganisms has recently become a topic of interest. The presence of oxygen atoms makes GO superior to pristine

Published on 05 Waysu 2018. Downloaded on 01/08/2024 7:53:25 AM.

Table 1 Comparison of antibacterial properties of GO, C-Dots, and some important antibacterial metallic and metal oxide NPs

	Nanoparticle	Size	MIC	Bacteria used for the study	Mode of action	Ref.
Metallic NPs	Ag NPs	10 nm	30 μg mL^{-1} 80 μg mL^{-1} 20 μg mL^{-1}	*E. coli* *S. aureus* *B. subtilis*	Penetration through bacterial cell wall and cell membrane damage, and ROS generation	151
	Au NPs	25 nm	200 μg mL^{-1}	*Corynebacterium pseudotuberculosis*	Penetration through cell wall, forming agglomerates	152
	Au nanoclusters	<2 nm	n/a	*E. coli* *S. aureus*	ROS generation. More negatively charged surface preserve the generated ROS, leading to higher ROS level	19
Metal oxide NPs	CuO	40 nm	n/a	*Photobacterium phosphoreum*	Release of Cu ions and the particulates of CuO	17
	Fe_2O_3	n/a	0.1 μg mL^{-1}	*E. coli*	ROS generation	153
	ZnO	17–30 nm	n/a	*S. aureus*	ROS generation (superoxide assisted ROS generation under dark)	154
	TiO_2	40–250 nm	10 wt%	*E. coli*	Photoactivation of TiO_2 causing peroxidation of polysaturated phospholipid of the cell membrane, leading to bacterial death	155
GO	GO nanosheets	Few nanometers	85 μg mL^{-1}	*E. coli*	Cellular damage due to oxidative stress	48
	GO	Few micrometers	250 μg mL^{-1}	*K. pneumoniae* *E. coli* *P. aeruginosa*	ROS generation	49
	GO	0.525 μm	150 μg mL^{-1}	*P. aeruginosa*	ROS generation	50
	GO nanosheets	nm–μm range	80 μg mL^{-1}	*S. mutans* *P. gingivalis* *F. nucleatum*	Cellular damage and leakage of cytoplasm	51
	GO nanosheets	0.31 ± 0.20 μm	80 μg mL^{-1}	*E. coli*	Cell membrane rupture due to direct contact, wrapping	53
	GO nanosheets	n/a	n/a	*E. coli* *S. aureus*	Cell membrane rupture due to direct contact	54
	GO nanosheets	n/a	0.05 mg mL^{-1}	*P. putida*	Loss of membrane integrity due to sharp edges of GO	56
	GO	Few micrometers	n/a	*E. coli*	ROS generation and light induced electron transfer	59
C-Dots	Spermine C-Dots	2.69 nm (ζ = +27.6 mV)	300 μg mL^{-1}	*E. coli*	ROS generation	32
	Spermidine-capped fluorescent C-Dots	~4.6 nm (ζ = +60.6 mV)	0.9 μg mL^{-1}	*E. coli* *S. aureus* *B. subtilis* *P. aeruginosa*	Disruption of cell membrane by multivalent interaction C-Dots with cell membrane	89
	Spermidine C-Dots	~6 nm (ζ = +45 mV)	2–4 μg mL^{-1}	*E. coli* *S. aureus* *P. aeruginosa*	Cell membrane rupture by multivalent interaction of C-Dots with cell membrane	90
	Quarternized C-Dots	~4 nm (ζ = −16 mV)	8 μg mL^{-1}	*S. aureus*	Cell membrane rupture by electrostatic interaction of C-Dots with cell membrane	92
	Multifunctional fluorescent magneto-C-Dots	~40 nm (ζ = +50 mV)	n/a	*S. aureus* *Salmonella*	ROS generation and membrane disruption	93

ζ: zeta potential; n/a: not available.

This journal is © The Royal Society of Chemistry 2019

Published on 05 Waysu 2018. Downloaded on 01/08/2024 7:53:25 AM.

graphene for various applications. The antibacterial activity of graphene-based nanomaterials was first reported by Fan *et al.*,[48] while the GO nanosheets exhibit no significant cytotoxicity to adenocarcinomic human alveolar basal epithelial cells (A549) at a low concentration of 20 μg mL^{-1}.[48] The viability of bacteria in the presence of GO-based nanomaterials is determined by the nature of GO, incubation time, and nanomaterial concentration.[49–52] Chen *et al.* found that bacterial inactivation typically occurs in the first hour of incubation and the rate of cell death increases with GO concentration.[52] This study also demonstrated that the antibacterial activity of GO increases with the lateral size. Yang *et al.* reported that bare GO has an intrinsic antibacterial activity in saline due to the presence of basal planes.[47] The *in vitro* and *in vivo* studies by Zhao *et al.* showed that GO inhibits the growth of *K. pneumonia*, thereby increasing the survival rate of mammalian lung cells; reducing tissue damage; decreasing inflammation of various organs; and decreasing the mortality rate of mice.[49] The studies suggest that GO can be a promising nanomaterial against multidrug-resistant (MDR) pathogens. However, bacterial infection could recur after the treatment with GO, compared to the mock-treated mice, suggesting different antimicrobial activities of graphene materials between *in vitro* and *in vivo* cases. Therefore, an in-depth understanding of the antibacterial mechanism and various environmental conditions affecting the antibacterial properties and cytotoxicity toward mammalian cells is needed to derive more effective antibacterial GO-therapeutics.

2.1 Antimicrobial mechanism of GO

In general, the development of antimicrobial activity for graphene-based nanosheets (including graphite, graphite oxide, GO, and rGO) proceeds in three steps: (1) deposition of nanosheets on the bacterial surface, (2) membrane disruption by sharp nanosheets, and (3) the ensuing superoxide anion-independent oxidation.[53] The level of antibacterial activity can be synergistically enhanced by membrane stress and oxidative stress. The stresses induced by GO lead to a stronger antibacterial activity, compared to rGO and graphite. Specifically, the antibacterial activity of GO arises from various physical or chemical interactions between GO and bacterial cell (Fig. 1).[54] During the physical interaction, the sharp edges of the GO nanosheets damage cell membrane.[54] Hydrazine-reduced GO nanosheets possessing sharper edges can effectively mediate charge transfer between bacterial cells and thus show a higher antibacterial activity.[54] Because the damage to cell membrane is caused by direct contact of GO with the cell, Gram-negative bacteria with an outer membrane are more resistant to such a damage than Gram-positive bacteria. Molecular dynamics simulation on graphene nanosheets revealed that the nanosheets penetrate cell membrane spontaneously within a few nanoseconds when they align vertically at a distance of 3.5–4.7 nm from the membrane surface.[55] This insertion occurs in three modes: *i.e.* (1) the swing mode, in which the nanosheets contact the membrane surface multiple times; (2) the insertion mode, in which the membrane traps nanosheets by van der Waals forces and hydrophobic interactions, followed by membrane cutting; and (3) the extraction mode, which leads to deformation and loss of membrane integrity.[55] Some bacteria, such as *Pseudomonas putida*, lose membrane integrity in the presence of GO nanosheets, but their metabolic activity is unaffected.[56] GO can also develop an antimicrobial activity to phytopathogens (such as *Pseudomonas syringae*, *Xanthomonas campestris pv. undulosa*, *Fusarium graminearum*, and *Fusarium oxysporum*) through mechanical wrapping of the cell membrane, resulting in membrane

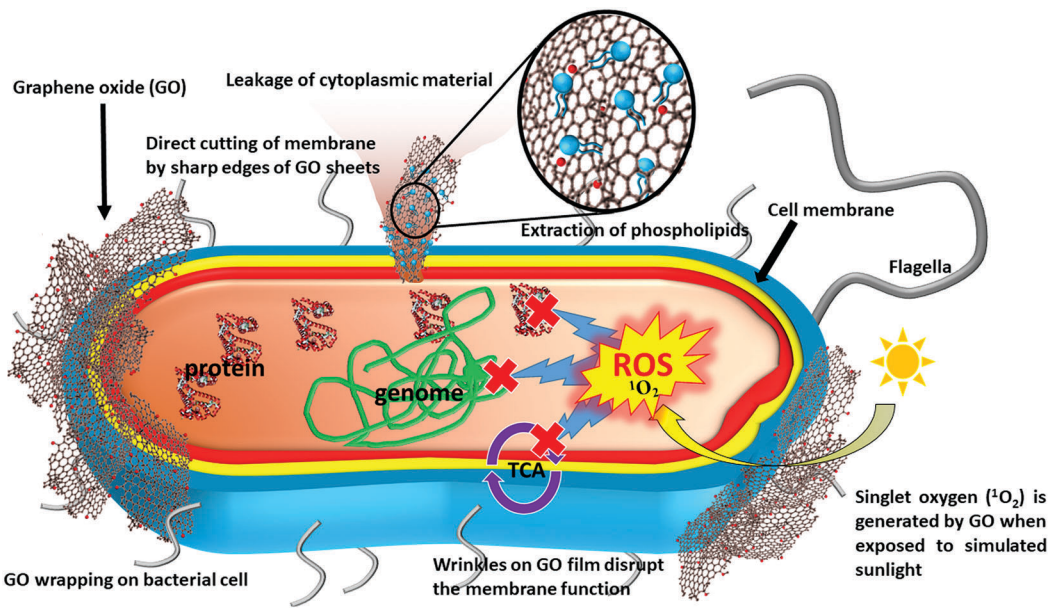

Fig. 1 Antimicrobial activity mechanism of GO through various physical and chemical interactions: including bacterial cell damage by the sharp nanowall/edge of GO, extraction of phospholipids, wrapping of bacterial cell by large-surface-area GO, ROS generation for disruption of genomic DNA, proteins and cellular metabolism (represented by TCA), and wrinkles in the GO film for membrane disruption.

Published on 05 Waysu 2018. Downloaded on 01/08/2024 7:53:25 AM.

damage and cell lysis.[57] In some cases, the mechanical wrapping might not necessarily affect the metabolic activity.[58]

On the other hand, the chemical damage is initiated by the formation of ROS and/or charge transfer, subsequently resulting in oxidative stress.[55] The stress on the membrane can induce fragmentation of genomic DNA and cell death.[50] Chong *et al.* demonstrated the enhanced antibacterial activity of GO when exposing it to simulated sunlight, which may result in the formation of ROS along with light-induced electron-hole pairs.[59] This study also reported that singlet oxygen ($^1O_2$) is the only type of ROS generated by the sunlight-exposed GO, though it only slightly contributes to the antibacterial activity relative to the simultaneously generated electron-hole pairs. It is suggested that the light irradiation could accelerate electron transfer from the innate antioxidant systems of *E. coli* to GO, thereby destroying key biomolecules such as glutathione (GSH), which ordinarily protects cells from oxidative stresses. In addition, the light irradiation may also reduce GO, resulting in the formation of carbon-centered free radicals to augment the antibacterial activity.[59]

2.2 Factors affecting the antibacterial nature of GO

As described above, GO has different antibacterial mechanisms, including mechanical cutting of cell membrane, wrapping of cell, ROS generation, and extraction of cellular materials. Several intrinsic characteristics of GO nanomaterials, such as conductivity, catalytic activity, and level of the interaction with biomolecules, are highly dependent on their morphological, physical, and chemical properties, including lateral size, purity, structural defects, charge, functional groups, degree of oxidation, and hydrophilicity. Therefore, all these factors contribute to the overall antibacterial activity of GO (Fig. 2).[60] Note that most antibacterial GO nanomaterials are characterized in a simple aqueous solution, whereas their practical applications are conducted in a multicomponent medium, leading to contradicting results and, therefore, engendering the need for more *in vivo* studies to reveal the actual antibacterial potency and mechanism.

2.2.1 Size. The antibacterial ability of GO nanosheets, specifically related to the effectiveness of cell adhesion, cell intake, and cell damage caused by the interaction between GO and cell, is highly influenced by the lateral size of GO.[61] A study by Elimelech *et al.* revealed that GO nanosheets with a small lateral size exhibit antimicrobial effects mainly through the oxidative stress, which is related to the defect density of the nanosheet, whereas GO nanosheets with a large lateral size exhibit antimicrobial effects through the cell entrapment mechanism.[61] Therefore, small-lateral-sized GO has a higher antibacterial activity specifically in the form of surface coating, whereas large-lateral-sized GO has a high antibacterial activity in the form of suspension. A study by Chen *et al.* showed the lateral-dimension-dependent antibacterial activity of GO in the form of suspension.[52] They reported that the viability of *E. coli* decreased by 98%, 92%, 88%, 72%, 61%, and 46% after incubating in aqueous suspensions with GO with lateral sizes of 0.753, 0.127, 0.065, 0.035, 0.013, and 0.010 μm^2, respectively. The large-lateral-sized GO nanosheets could highly wrap bacterial cells, thereby preventing them from medium access and leading to their death. This study also showed that the time- and concentration-dependent antibacterial activity of GO nanosheets with a large lateral size primarily depends on their direct interaction with the cell rather than the degree of oxidation or aggregation.

2.2.2 Morphology. The morphological effects are associated with both GO nanomaterial and bacterial cell. The physical structure and nanoscale geometry of GO affect its interaction with bacteria. GO films with surface wrinkles show excellent antibacterial properties due to the corrugated nature at the nanometric level.[62] Lee *et al.* showed that wrinkled GO surfaces are more effective than planar surfaces in terms of inducing the interaction with cell materials and driving the alteration of cell alignment, orientation and morphology.[63] Wrinkled GO can reduce bacterial viability and, therefore, show an excellent antibacterial activity within a short period of 15 min of its adminstration.[62] Wrinkled GO nanosheets with a high surface roughness can pierce the peptidoglycan layer for membrane damage. When trapped by the nano-grooves of the wrinkled GO surface, bacterial cells could experience oxidative stress, resulting in membrane rupture and release of intracellular components (Fig. 3). The antibacterial activity of GO can be

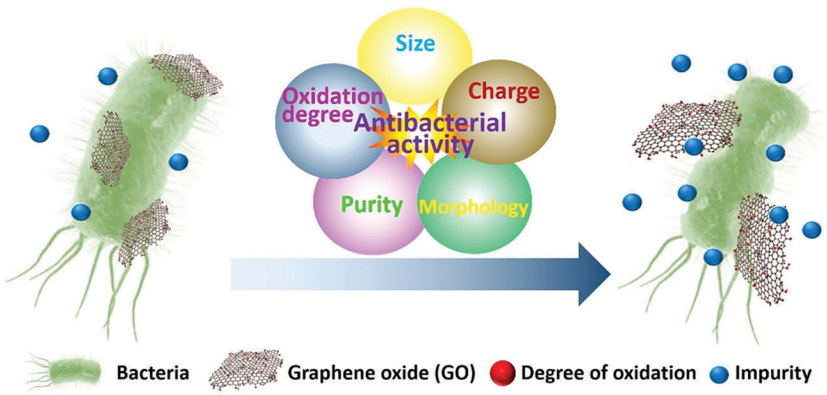

Fig. 2 Factors affecting the antibacterial properties of GO.

 This journal is © The Royal Society of Chemistry 2019

Published on 05 Waysu 2018. Downloaded on 01/08/2024 7:53:25 AM.

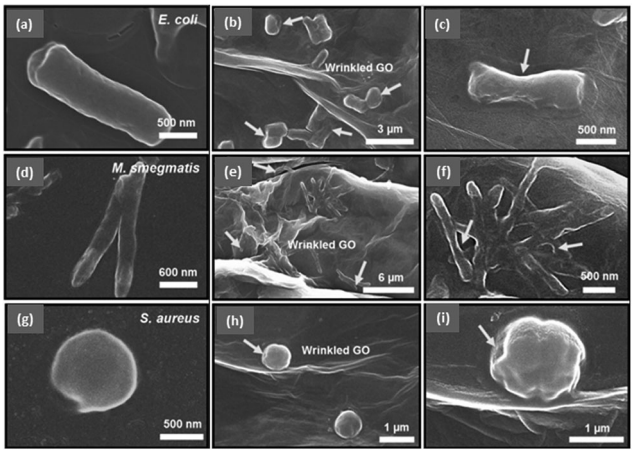

Fig. 3 Scanning electron microscope (SEM) images of (a–c) rod-shaped *E. coli*, (d–f) rod-shaped *M. smegmatis*, and (g–i) spherically shaped *S. aureus* before (a, d, and g) and after (the others) the treatment with wrinkled GO surfaces. The arrows point to the spots of disruption of the cell membrane caused by the exposure to wrinkled GO films. Reproduced from ref. 62 with permission. Copyright (2016) American Chemical Society.

also affected by the biological morphology, specifically the structural nature of cell membrane. Gram-positive bacteria possess a thick peptidoglycan layer of 20–80 nm, whereas Gram-negative bacteria possess a much thinner layer of approximately 2–3 nm. As a result, Gram-negative bacteria are highly prone to the attack by GO nanosheets, compared to Gram-positive bacteria.[51]

2.2.3 Aggregation. The interaction between GO and bacteria (*E. coli* and *S. aureus*) significantly depends on GO concentration, charge, dispersibility, and aggregative state in different solutions (deionized water, phosphate-buffered saline, NaCl, $MgCl_2$, and $CaCl_2$ solutions), leading to varying antibacterial effects.[64] Palmieri *et al.* reported that GO at low concentrations (<6 μg mL^{-1}) exhibits strong antibacterial effects in all solutions. The non-aggregated GO mechanically disrupts bacterial membrane, resulting in the leakage of intracellular materials and eventually cell death. Interestingly, increasing the GO concentration causes different outcomes. GO appears to be structurally stable in deionized water at a concentration up to 200 μg mL^{-1} (highest concentration tested in their work), within which the antibacterial ability increases with the GO concentration. On the other hand, in the presence of salts, GO forms different sized aggregates depending on the GO concentration and cation type. At medium concentrations (25–50 μg mL^{-1}), GO tends to cluster by forming floating scaffolds in a saline solution, resulting in the enhancement of bacterial growth. However, increasing the concentration of GO above 50 μg mL^{-1}, will mediate the formation of large GO aggregates and their tight attachment with bacterial membrane in the presence of divalent cations such as Mg^{2+} and Ca^{2+}. As a result, the large GO clusters tend to wrap bacterial cells and impede bacterial growth.[64]

2.2.4 Degree of oxidation. The reports on the effects of degree of oxidation on the antibacterial activity of GO are contradictory.[50,59,65] Buccheri *et al.* showed that, the flake size of GO decreases and exhibits an enhanced antibacterial activity toward *E. coli* when the GO is irradiated with a pulse laser for 3 h, while the material is non-toxic toward zebrafish.[65] However, the oxygen content and hydrophilicity of GO are preserved upon the laser irradiation. On the other hand, upon exposure to simulated sunlight, GO is converted to rGO with an enhanced antibacterial activity toward *E. coli*.[59] The enhanced antibacterial activity is associated with the formation of carbon-centered free radicals, accelerating electron transfer. However, Gurunathan *et al.* reported that the antibacterial ability against *P. aeruginosa* is reduced when GO is chemically reduced by hydrazine, presumably due to reduced ROS generation and less effective DNA fragmentation.[50]

2.2.5 Basal plane. Reports documenting the effects of GO on bacterial growth have been controversial.[49,65,66] Yang *et al.* explained these contradictory reports based on different experimental conditions during the analysis.[47] In general, the bacterial killing assays or antibacterial experiments are conducted in saline or buffer solutions with no nutrients, while the bacterial growth inhibition assays are studied in nutrient broths. The report by Yang *et al.* suggests that though GO nanosheets are antibacterial in saline solutions, gradual supplementation of Lysogeny broth (LB) deactivates the antibacterial activity. Even up to 10% LB broth supplementation is sufficient to inactivate the antibacterial ability of GO.[47] However, increasing the concentration of GO recovers the antibacterial activity. They suggest that deactivation of the antibacterial activity of GO may be due to the nonspecific adsorption of some medium components onto the basal planes of GO. Thus, it is proposed that the antibacterial ability of GO depends on the availability of the basal plane for interaction with bacterial cells.[47] They further reported that bare GO exhibits cytotoxicity toward mammalian cells, and the cytotoxicity decreases when the basal planes are masked by the non-covalent adsorption.[47] Their report is further supported by Advincula *et al.*, who claim that the primary factor contributing to the antimicrobial activity of GO is its basal plane rather than the edge, based on the studies on GO sheets immobilized on polyethylene terephthalate (PET) substrates by the Langmuir–Blodgett (LaB) technique to form GO-LaB films.[67] The antibacterial activity of the GO-LaB film increases with the number of layers, where GO lies flat on the substrate, contributing more basal plane rather than sharp edge.

2.2.6 Purity. Though many factors affecting the antibacterial activity of GO have been identified, the purity effect is rarely reported. Roberts *et al.* demonstrated that the presence of impurities may mask the actual effect of GO in biological systems.[68] The authors demonstrated that while the commercial GO exhibits antibacterial properties against *E. coli*, it becomes neutral after further purification by thorough washing with deionized water.[68] Neither cell morphology nor cell membrane is affected in the presence of purified GO. They also reported that the lateral size of GO has a negligible effect on bacterial growth under this condition. The study suggests that poorly purified GO exhibits antibacterial properties potentially due to the presence of certain acidic and small impurities. However, the neutralized antibacterial activity of purified GO may also be associated with the aggregation of GO during the purification.

Published on 05 Waysu 2018. Downloaded on 01/08/2024 7:53:25 AM.

2.2.7 Composites. As reviews on the antibacterial mechanism of graphene-based composite nanomaterials have been published,[69,70] we briefly describe recent antibacterial application of GO-based composites. Besides the suspension form, graphene-based nanomaterials in a membrane form also exhibit antibacterial properties. For example, GO and rGO in a paper form prepared by vacuum filtration possess excellent antibacterial properties against *E. coli*.[48] Two-dimensional GO nanosheets with antibacterial properties can be fabricated into thin composite membranes for treating water-containing biological wastes. GO-incorporated polyamide membranes show a superior antibacterial activity over pure polymeric membranes, and the activity increases with the concentration of GO.[71] Tannic acid-functionalized GO crosslinked with hyper-branched polyethyleneimine exhibits a high performance in bacterial inactivation, due to the synergistically enhanced antibacterial activity of GO and tannic acid.[72] GO dispersed in a polyvinyl-*N*-carbazole (PVK) matrix with a weight ratio of 97 : 3 (PVK : GO) shows an excellent antibacterial activity against both Gram-negative (*E. coli* and *Cupriavidus metallidurans*) and Gram-positive (*Bacillus subtilis* and *Rhodococcus opacus*) bacteria.[58] Surface modification of commercial cellulose nitrate membrane filters with a selection of graphene-based materials has been shown to improve the membrane's antibacterial activity.[73] The production of ROS by GO-based nanocomposites contributes to the enhanced antibacterial activity of the modified filters. Elimelech *et al.* found that a GO-modified polyamide membrane shows enhanced antibacterial properties while maintaining an effective membrane performance.[74] GO-modification can enhance the antibacterial activity not only for polymeric membranes but also bacterial cellulose nanocomposite membranes.[75] Crosslinking GO with chitosan at 120 °C can enhance the mechanical strength and antibacterial activity of the chitosan nanocomposite film, making it more suitable for food packaging applications.[76] Though GO is hydrophilic, the hydrogen bonding and electrostatic attraction between chitosan and GO do not alter the hydrophobicity of the resulting polymer. A thorough review on the antibacterial effects of GO-based antibacterial polymeric membranes has been published.[77]

In addition to GO–polymeric composites, GO–metal and GO–metal-oxide composites also show a promising antibacterial activity, which can be attributed to both GO and metal and/or metal-oxide moieties.[78] Due to the enhanced antibacterial nature and unique molecular affinity/specificity, GO–metal/metal-oxide nanocomposites, such as GO–Ag, GO–Fe_2O_3, GO–ZnO, have various applications, including wound dressing, oral pathogen killing, organic dye removal, water purification, furnishing and decoration.[79–83] GO–Ag nanocomposites show a synergistically enhanced antibacterial activity against *E. coli* and *S. aureus*, compared to individual GO or Ag nanoparticles.[79,80,82] Propagation of nosocomial pathogens, such as *Salmonella typhimurium* and *Staphylococcus epidermidis*, can be inhibited by rGO–WS_2 nanocomposite *via* elevated oxidative stress for membrane disruption.[84] The antibacterial activity is dependent on the concentration of rGO–WS_2 and incubation time. GO–Ag nanocomposites, when administered with tobramycin, can be applied to combat MDR bacteria through combined antibacterial effects of GO (mediating cell wall disruption), Ag (mediating an elevated intracellular oxidative stress), and tobramycin (mediating the inhibition of protein synthesis in bacteria).[85] In addition to GO-based composites, coating of GO on a supporting metal substrate, such as Zn, Ni, Sn, and steel, can enhance electrical conductivity since GO on the metal substrate can act as an electron pump to accelerate the electron transfer. The charge transfer from cell membrane to oxygen-containing functional groups on the surface of GO induces the formation of ROS, which compromises bacterial metabolism and membrane structure, resulting in an enhanced antibacterial activity.[86]

3. Antimicrobial activity of C-Dots

C-Dots have attracted great attention for biomedical applications in recent years due to their easy synthesis, tunable fluorescence, low cytotoxicity, and high biocompatibility.[21,24,29] C-Dots, including carbon quantum dots (CQDs; sp^2/sp^3 carbon) and graphene quantum dots (GQDs; sp^2 carbon), can be functionalized with different molecules and functional groups for biolabeling, sensing, tissue imaging, and antibacterial applications.[21,24,29] C-Dots can be synthesized by both bottom-up and top-down approaches.[24,29] Bottom-up synthesis is preferred due to the high synthetic diversity from miscellaneous precursors and easy functionalization with desired functional groups. By controlling the surface charge and functional properties, the affinity, specificity, and antibacterial properties of the C-Dots can be manipulated.[21,29,30,87,88] We recently reported the synthesis and surface modification of a variety of C-Dots from different precursors for various applications, including bacterial labeling and bacterial inactivation (even for MDR bacteria).[30,31,89,90] Moreover, C-Dots surface-passivated with various molecules, such as 2,2′-(ethylenedioxy)bis (ethylamine) and 3-ethoxypropylamine, have been reported to possess antiviral properties.[44]

3.1 Antimicrobial mechanism of C-Dots and factors affecting antibacterial activity

C-Dots inhibit bacterial growth or kill bacteria through complex mechanisms, including ROS generation, disintegration of cell structure, fragmentation and condensation of genomic DNA, leading to the leakage of the cytoplasm.[32,89–91] The antibacterial ability of C-Dots can be highly associated with the surface charge and generation of ROS. For example, we recently reported the synthesis of spermidine-functionalized carbon quantum dots (Spd-CQDs) with plenty of positive charges (zeta potential up to +60.6 mV) on the surface.[89] The Spd-CQDs exhibit a multivalent interaction with the negatively charged bacterial membrane and cause severe damage to the membrane and leakage of the cytoplasm.[89] In addition, the Spd-CQDs at a low concentration can interact with nucleic acids, such as plasmid DNA and small interfering RNA, resulting in modulation of gene expression. Though various factors associated with the antibacterial activity of Spd-CQDs have been identified, reports regarding the involvement of ROS generation have been

 This journal is © The Royal Society of Chemistry 2019

Published on 05 Waysu 2018. Downloaded on 01/08/2024 7:53:25 AM.

controversial. A study by Bing *et al*. showed that positively charged spermine-functionalized CQDs exhibit antibacterial activity against *E. coli* mainly through generation of ROS, though membrane disruption through electrostatic interaction is also observed.[32] However, ROS-induced from the Spd-CQDs does not appear to occur according to our observation.[89]

3.1.1 Charge on C-Dots. The nature and level of the charge on C-Dots can critically affect their interaction with bacterial cell membrane. Bing *et al*. reported the synthesis of positively charged, negatively charged, and neutral C-Dots from spermine, candle soot, and glucose, respectively. However, each one of them interacts differently with bacterial cell membrane.[32] They observed that positively charged C-Dots exhibit a decent level of antibacterial ability, negatively charged C-Dots are bacteriostatic, whereas neutral C-Dots are hardly active toward *E. coli*.[32] Moreover, they reported that ROS generation induced by positively charged C-Dots is higher than that induced by negatively charged ones, and neutral ones hardly induce ROS generation. However, a direct relation between surface charge and ROS generation has not been identified. Dou *et al*. reported a superior antibacterial activity (against both Gram-positive and Gram-negative bacteria) for multifunctional C-Dots, prepared from glucose and poly(ethyleneimine) (PEI) followed by quaternization with benzyl bromide, though the synthesis time is as long as 12 h.[87] With positive surface charges, the quaternized C-Dots can adhere to bacterial cell membrane for disruption of it.

3.1.2 Functional groups on C-Dots. The functional groups on C-Dots highly influence antibacterial properties. For example, amine-functionalized C-Dots modified with lauryl betaine can possess both antibacterial and bacterial differentiation abilities, resulting in selective fluorescence labeling and killing of Gram-positive bacteria in a mixture of Gram-positive and Gram-negative bacteria (Fig. 4A).[92] Positively charged quaternized C-Dots with a long and multicolor fluorescence emission can differentiate Gram-positive (*S. aureus*) and Gram-negative bacteria (*E. coli*) by selectively attaching to Gram-positive bacteria. Additionally, the minimum inhibitory concentration (MIC) of the quaternized C-Dots can be significantly reduced, as low as 8 μg mL^{-1} toward *S. aureus*. The presence of both hydrophobic hydrocarbon chains and positively charged quaternary ammonium groups enables the selective attachment of the C-Dots to Gram-positive bacteria for bacterial differentiation and inhibition.[92] The cell surfaces of *S. aureus* get damaged and wrinkled, and a leakage of intracellular contents occurs after incubation with the quaternized C-Dots for 2.5 h (Fig. 4B).

In addition to antimicrobial applications, fluorescent C-Dots can be used for bacterial identification and separation from contaminated blood samples when attached to magnetic nanoparticles.[93] Ray *et al*. demonstrated that a conjugated system of pardaxin antimicrobial peptides and magneto-C-Dot nanomaterials could be used for the diagnosis, separation, and disinfection of pathogens, even at an early stage of the infection.[93] The pore-forming pardaxin exhibits an antibacterial activity *via* induced formation of ROS, and the level of the activity can increase when pardaxin is conjugated with magneto-C-Dots. Notably, this conjugated system can exhibit a promising antibacterial activity toward MDR bacteria, such as methicillin-resistant *S. aureus* (MRSA), with an MIC at 1.8 μg mL^{-1}. More recently, nitrogen-doped GQDs functionalized with amino groups are reported to possess a superior ability to produce photo-induced ROS than that of unmodified GQDs, resulting in an improved antibacterial activity.[94] Jijie *et al*. reported that amine-functionalized C-Dots can be used as a carrier for the delivery of antibiotics, such as ampicillin.[95] Compared to free ampicillin, the immobilized ampicillin on the C-Dots surface has a higher stability. In addition, the ampicillin-modified C-Dots show an effective killing of *E. coli* cells as a result of the combined antibacterial function of ampicillin and photodynamic effect of C-Dots.

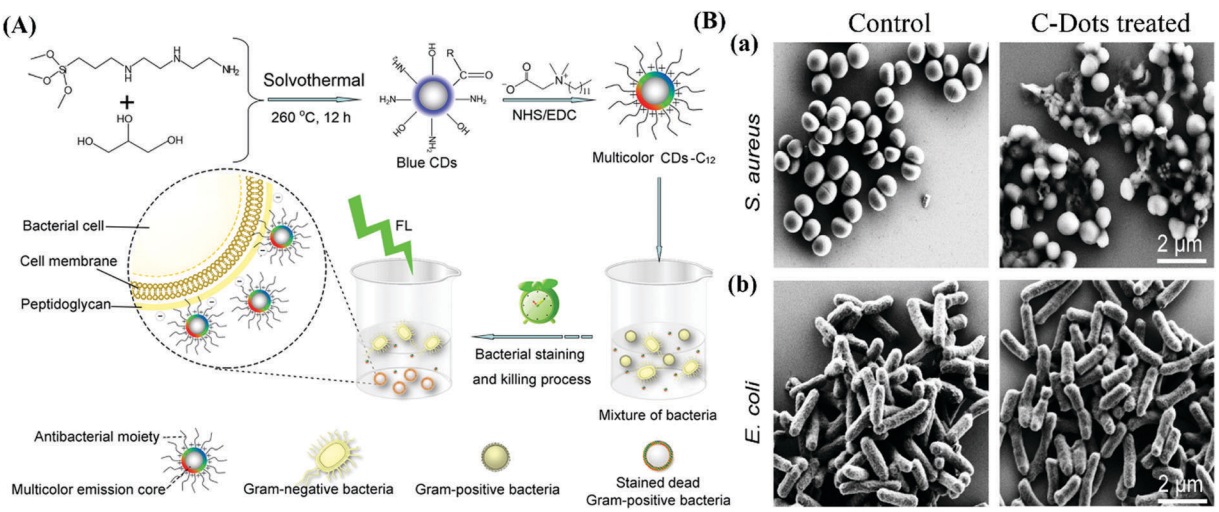

Fig. 4 (A) Schematic representation of the strategy for the synthesis of amine-functionalized C-Dots modified with lauryl betaine for selective labeling and inhibition of Gram-positive bacteria in a mixture of Gram-positive (*S. aureus*) and Gram-negative (*E. coli*) bacteria. (B) SEM images of *S. aureus* (a) and *E. coli* (b) cells without (control) and with the treatment of the quaternized C-Dots. Reproduced from ref. 92 with permission. Copyright (2016) American Chemical Society.

Published on 05 Waysu 2018. Downloaded on 01/08/2024 7:53:25 AM.

3.1.3 Shape and size of C-Dots. Hui *et al*. revealed how the shape and the source material of GQDs affect the antibacterial activity.[96] GQDs synthesized by rupturing C_{60} cages (*i.e.*, C_{60}-GQD) with a nonzero Gaussian curvature exhibit excellent antibacterial properties specifically against *S. aureus*, but remain inactive against other bacteria, such as *B. subtilis*, *E. coli* and *P. aeruginosa*.[96] The antibacterial activity of C_{60}-GQD depends on its interaction with the bacterial cell membrane for membrane disruption. The match in the surface curvature of GQD with the cell surface plays an important role for their interaction. The species-specific activity of C_{60}-GQD is also time- and dose-dependent. For example, the MIC of C_{60}-GQD for *S. aureus* is *ca.* 400 μg mL^{-1}, whereas C_{60}-GQD appears to be non-toxic to human cell-line HepG2 at a concentration up to 200 μg mL^{-1}.[96] In contrast, GQD prepared from GO (*i.e.*, GO-GQD) with a planar geometry and zero Gaussian curvature lacks antibacterial properties, even though both types of GQDs exhibit similar sizes, surface charges, and compositions. However, C_{60}-GQD and GO-GQD are different in the zeta potential, functional group, and oxygen/carbon (O/C) ratio. Thus, the specific structural factors determining the antibacterial activity of GQDs should be investigated further.

Su *et al*. reported the size-dependent antibacterial activity of GQDs against *E. coli*.[97] Small-lateral-sized GQDs, due to its small size at 15 nm, can easily penetrate the plasma membrane and causes more oxidative stress and membrane rupture than large-lateral-sized GQDs at 50 nm. The membrane disruption and oxidative stress can be associated with the ROS generation mediated by these GQDs.

3.2 H_2O_2- and light-assisted antimicrobial activity of C-Dots

While H_2O_2 is a common medical reagent to prevent bacterial infection, a high concentration, which may be harmful to tissue, is needed for disinfection. Qu *et al*. reported that H_2O_2 can be converted to the •OH radical, which has a higher antibacterial activity, in the presence of GQDs due to the peroxidase-like activity of GQDs.[98] In the presence of GQDs (100 μg mL^{-1}), the viability of *E. coli* and *S. aureus* decreases significantly upon the addition of 1 mM and 10 mM H_2O_2, respectively, compared to the concentrations of H_2O_2 of 100 mM and 1 M, respectively required in the absence of GQDs.[98] On the other hand, the bacterial cell viability is also dependent on the GQD dose.

In addition to the physical interaction with bacterial cell membrane and ROS generation as potential antibacterial mechanisms, certain functional C-Dots exhibit antibacterial activity through the photodynamic effect.[99,100] Trajkovic *et al*. reported such photodynamic effect for GQDs prepared by an electrochemical method.[100] The GQDs, when irradiated at 470 nm, can induce photodynamic toxicity to *S. aureus* and *E. coli* through ROS generation. The antibacterial activity of irradiated GQDs is dependent on the concentration of GQD and photo-exposure time, whereas GQDs without light exposure do not kill bacteria. More recently, Stanković *et al*. demonstrated that the photo-generation of singlet oxygen species by LaB films of hydrophobic CQDs derived from polyoxyethylene–polyoxypropylene–polyoxyethylene block copolymer Pluronic F-68 on a substrate (SiO_2/Si, glass, or mica) when irradiated with blue light (470 nm) mediates a superior antibacterial and antifouling activity.[101]

ROS generation mediated by GQDs may couple with two-photon excitation (TPE), based on which GQDs are photo-excited by two photons with the same or different wavelengths.[102] As the excitation wavelengths are longer than the emission wavelengths, TPE serves as an enhanced photodynamic therapy for bacterial killing with ultra-low energy levels and short photo-excitation periods. TPE-based photodynamic therapy (PDT) has attracted great interests due to its effective penetration ability into biological tissues with a minimum damage to adjacent healthy tissues and reduced photo-bleaching. Photo-excited GQDs can thus be used not only to eliminate MDR bacteria but also as a two-photon contrast agent for in-depth observation of 3-dimensional biological specimens. Recently, Sun *et al*. reported that C-Dots functionalized with 2,2′-(ethylenedioxy)bis-(ethylamine) (EDA) through amidation can serve as an effective antibacterial agent under photo-illumination.[99] The antibacterial activity of the EDA-functionalized C-dots (EDA-C-Dots) can be induced by visible light or even under ambient room-lighting conditions. The authors suggest that the photo-excitation of EDA-C-Dots causes charge separation on the surface of the C-Dots, and the resulting emissive excited states are likely associated with the observed antibacterial function. Recently, another effect on the photo-activated antibacterial ability of EDA-C-Dots, *i.e.* the fluorescence quantum yield, was also identifed.[103] The photo-activated antibacterial activity of EDA-C-Dots increases with the quantum yield, and is also dependent on photo concentration and exposure time. However, the effects of oxidative stress and ROS generation were not determined. Various other factors, including surface passivation (surface functional groups and charge), electron conductivity, and charge separation should also be investigated for thorough understanding of the photo-activated antibacterial mechanism.

3.3 Biomedical application of C-Dots

While various C-Dots have been synthesized and surface-modified for *in vitro* evaluation of their antibacterial activity, it is the *in vivo* studies that critically determine the suitability and effectiveness of these C-Dots for practical applications. We reported an *in vivo* application of spermidine-capped fluorescent carbon quantum dots (Spd-CQDs) prepared from ammonium citrate for the healing of MRSA-infected wound in rats (Fig. 5).[89] The antimicrobial and fluorescent Spd-CQDs with a diameter of ~4 nm are synthesized through pyrolysis of ammonium citrate in a solid state at 180 °C and then modified with spermidine by heating at 270 °C without a coupling agent. Structural characterization of the synthesized Spd-CQDs using X-ray photoelectron spectroscopy, Fourier transform infrared spectroscopy, elemental analysis, and laser desorption/ionization mass spectrometry reveals the deposition of spermidine and/or its pyrolytic molecules on the CQDs, resulting in Spd-CQDs that are rich in nitrogen (45%) and possess a high positive surface charge. The Spd-CQDs exhibit effective antibacterial activities against both non-MDR and MDR bacterial strains. Notably,

 This journal is © The Royal Society of Chemistry 2019

Published on 05 Waysu 2018. Downloaded on 01/08/2024 7:53:25 AM.

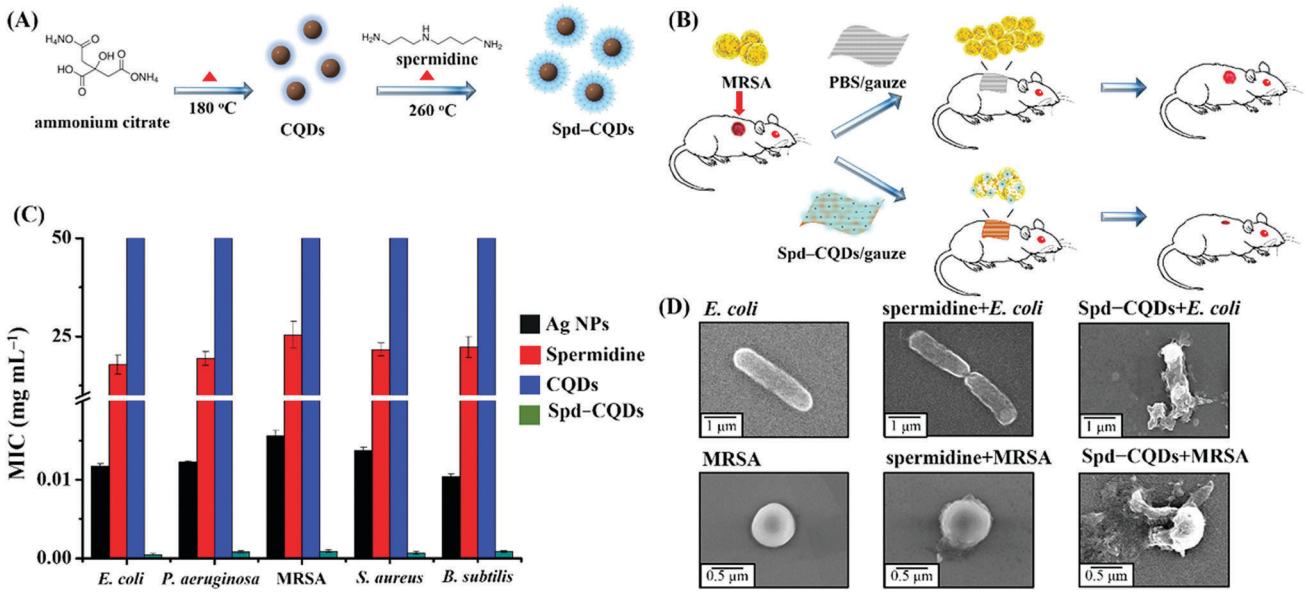

Fig. 5 Schematic representations of (A) the synthesis of Spd-CQDs from ammonium citrate and spermidine by a dry heating method and (B) *in vivo* application of Spd-CQDs for would healing in rat. (C) Comparison of MICs of Ag NPs, spermidine, CQDs, and Spd-CQDs against five bacteria. (D) TEM images of *E. coli* and MRSA cells before and after the treatment with spermidine or Spd-CQDs. Reproduced from ref. 89 with permission. Copyright (2016) Wiley-VCH Verlag GmbH & Co. KGaA, Weinheim.

the MIC of the Spd-CQDs at ~0.9 μg mL^{-1} for MRSA is less than 1/25 000 that of spermidine at ~26 mg mL^{-1} (Fig. 5C). While Spd-CQDs mainly cause structural damage to bacterial cell membrane (Fig. 5D), they are rather biocompatible. The *in vivo* experiments for the healing of MRSA-infected wound in rats demonstrated that Spd-CQDs are effective antimicrobial and wound healing agents, providing better epithelialization and production of collagen fibers. On the other hand, though C-Dots synthesized from different polyamines also show some antibacterial activity and wound healing effects, their effectiveness varies with the length of the polyamine and the surface charge of the synthesized CQDs.[89]

Qu *et al*. reported the efficiency of a GQD bandage in wound disinfection based on *in vivo* studies using Kunming mice.[98] Interestingly, GQD derived from GO does not exhibit any antibacterial activity *in vitro*. However, the intrinsic peroxidase-like activity of GQDs mediates the decomposition of H_2O_2 to generate •OH radicals with stronger antibacterial activity. This enables wound healing/disinfection using GQD bandages with a low concentration of H_2O_2.

The *in vivo* antibacterial activity of spermidine C-Dots (CQD_{Spds}, synthesized by the heating of spermidine in one-step) has been proved by the treatment of bacterial keratitis in rabbit eyes (Fig. 6).[90] Though silver nanoparticles (Ag NPs) are the most widely used antimicrobial nanomaterial with an MIC at 15–20 μg mL^{-1}, their high cytotoxicity is a concern due to the dissolution of silver ions. Based on the small size (~6 nm) and high surface charge (zeta potential of +45 mV), CQD_{Spds} are effective in disrupting bacterial cell membrane with an excellent biocompatibility, which have been proved by various *in vitro* and *in vivo* studies.[90] Furthermore, the positively charged CQD_{Spds} can serve as an effective eye drop medication to treat bacterial keratitis in rabbits (Fig. 6B).[90] While the *Staphylococcus*-infected rabbits treated with phosphate buffered saline (control) show a manifestation of bacterial infection during a 14-day follow-up, those in the CQD_{Spds}-treated group develop only mild tissue damage and ocular inflammation. In addition to the antibacterial activity, CQD_{Spds} can release the junction of corneal epithelial cells, enabling the penetration of therapeutics across the corneal epithelium for more effective treatment. The reduced treating concentration and side effects make CQD_{Spds} superior to the commercial antibiotic sulfamethoxazole (4%) eye drop that is widely used against Gram-positive and Gram-negative bacteria.

4. Cytotoxicity and biocompatibility

4.1 Graphene derivatives

Graphene-based nanomaterials show pulmonary, behavioral, reproductive, and developmental cytotoxicity, and even genotoxicity in laboratory mammals.[104] The cytotoxic effect of these nanomaterials to humans should be evaluated, as they may enter human body through respiration, skin absorption, gastrointestinal digestion, and injection, *etc*.[105] Having an excellent antibacterial ability, GO has been reported to be cytotoxic to mammalian cells at high concentrations (85 μg mL^{-1}).[48] GO nanosheets can damage or even penetrate mammalian cells with their sharp edges, resulting in cell death.[47] GO can damage DNA at a concentration of 10 μg mL^{-1} through an increased oxidative stress in the cell.[106] GO can be more cytotoxic than rGO toward human umbilical vein endothelial cells (HUVEC), and the cytotoxic effect increases with incubation time.[106] The lower cytotoxicity of rGO may be associated with structural

Published on 05 Waysu 2018. Downloaded on 01/08/2024 7:53:25 AM.

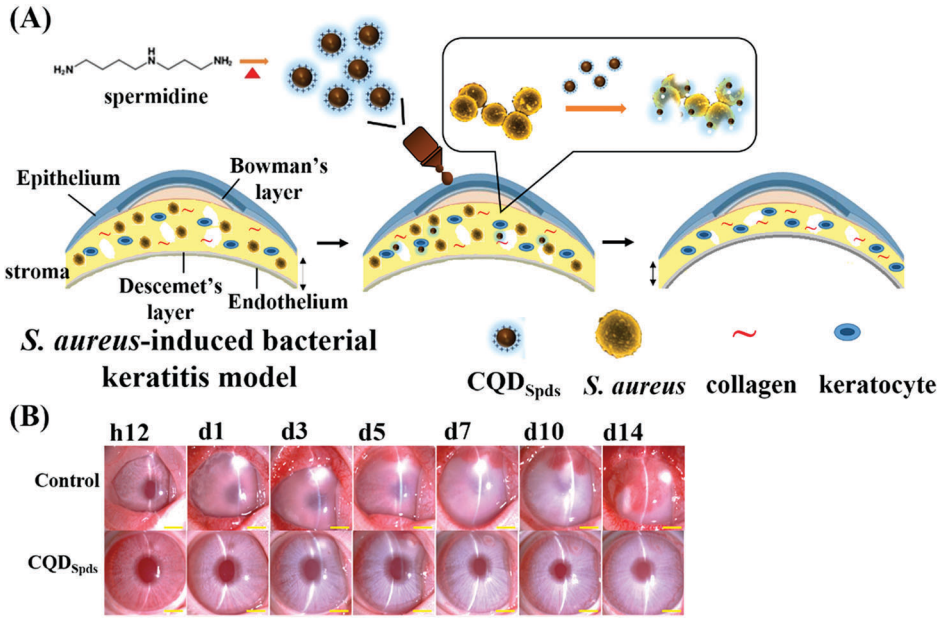

Fig. 6 (A) Schematic representation of the synthesis of CQD_{Spds} and *in vivo* application for the treatment of bacterial keratitis. (B) Time-course of the treatment showing the *in vivo* therapeutic efficacy of CQD_{Spds} after topical instillation in the eyes of a rabbit with bacterial keratitis. Reproduced from ref. 90 with permission. Copyright (2017) American Chemical Society.

agglomeration.[53,106] The cytotoxicity of small-lateral-sized GO and rGO is higher than that of large-lateral-sized ones due to their stronger interaction with the cell and, thereby, more ROS generation.[106] Basically, the surface chemistry of GO, such as the nature and density of the oxygenated functional group, critically affects the cytotoxicity.[106] A low level of the oxygenated functional groups can reduce oxidative stress and DNA damage.[106] On the other hand, the cytotoxicity can be reduced by non-covalent adsorption of small molecules on the basal plane of GO, thereby masking the basal plane.[47] The adsorption of proteins on the surface of GO can reduce the available surface area for interaction with cell membrane, thereby mitigating the cytotoxicity.[107,108] The *in vivo* cytotoxicity of GO is size- and dose-dependent.[109] While GO appears to be non-toxic in mice at doses up to 0.25 mg, increasing the dosage to 0.4 mg causes lung granuloma and affects the liver, spleen, and kidneys, and eventually causes 40–50% mice death.[110] Recently, Zhou *et al.* reported the adsorption of GO onto 20S proteasome, resulting in suppression of the proteolytic activity of proteasome.[111] This effect, through which cell cycle and survival can be disturbed, is dependent on GO dose and lateral size. The activity of 20S proteasome (2 μg mL^{-1}) can be completely inhibited by large-lateral-sized GO (0.5–3 μm) at 10 μg mL^{-1}. However, with the same dose, medium-lateral-sized GO (50–200 nm) causes ~50% suppression, and small-lateral-sized GO (<10 nm) does not show any suppression. This data is also consistent with the results based on molecular dynamics simulation. Another report showed that GO functionalized with poly(sodium 4-styrenesulfonate) accumulates in the body of mice for more than 6 months, and chronic inflammation of liver and lungs occurs at a high dosage (16 mg kg^{-1} body weight).[112] Kostarelos *et al.* reported that functionalized GO with a long term storage results in structural re-stacking, thereby increasing the thickness of the GO sheets. Around 47.5% of the injected dose of thicker GO sheets accumulate in the liver and spleen of mice, whereas 76.9% of the injected dose of thinner GO sheets get excreted through urine.[113] Wistar rats exposed to GO (with a thickness 0.8–2 nm and lateral dimension 5–10 μm) at a high concentration (10 mg per kg body weight) had a reduced sperm motility and increased sperm abnormality; however, a significant recovery was observed in 30 days.[114] Additionally, the sperm quality parameters appear to be unaltered by GO even after eight weeks of GO exposure by intratracheal instillation (18 mg per mouse) in another report.[115] The *in vitro* and *in vivo* antibacterial activities of GO are not necessarily related to each other. Though GO can be used as an effective antibacterial agent *in vivo* with minimal cytotoxicity to tissues and organs, a complete prevention of bacterial infection using GO has not been achieved. Hence, a thorough understanding of the mechanistic development of the antibacterial activity of these nanomaterials in animals is important before their wide use in clinical applications.

4.2 C-Dots

C-Dots not only possess antibacterial and antiviral properties, but also show an excellent biocompatibility. The excellent biocompatibility of C-Dots enables their applications in cell imaging, biolabeling, and antibacterial drug delivery.[21,24] We recently demonstrated that the hemolysis of human RBCs is insignificant in the presence of Spd-CQDs, even when the concentration of Spd-CQDs is 100-fold higher than the MIC for bacteria.[89] On the other hand, the CQD_{Spds} for treating bacterial keratitis has a negligible cytotoxicity toward rabbit corneal keratocytes (RCK cells), even though there is a structural interaction between CQD_{Spds} and RCK cells.[90] Additionally, CQD_{Spds} are

 This journal is © The Royal Society of Chemistry 2019

Published on 05 Waysu 2018. Downloaded on 01/08/2024 7:53:25 AM.

harmless to human RBCs at concentrations up to 100 μg mL^{-1} and do not cause any genotoxic or oxidative damage and hemagglutination. While the antibacterial activity of C-Dots depends on the surface charge which mediates their interaction with bacterial cell for membrane rupture, the plasma membrane of mammalian cells contains cholesterol which can strengthen the membrane and lower the membrane potential. Therefore, positively charged C-Dots exhibit a low cytotoxicity to mammalian cells, as opposed to their high antibacterial activity to bacterial cells.[89,90]

Tan *et al*. observed that the C-Dots derived from grilled fish exhibit a low cytotoxicity and high biocompatibility toward mouse osteoblast cells (MC3T3-E1), even at a high concentration of 20 mg mL^{-1}.[116] Zboril *et al*. reported the cytotoxic effects of the C-Dots derived from candle soot with different chemical groups for surface functionalization.[117] The *in vitro* cytotoxicity studies on mouse fibroblasts (NIH/3T3) reveal that the negatively charged C-Dots derived from candle soot can affect cell cycle (by arresting the G2/M phase) and cause a high oxidative stress, even though they do not enter the cell nucleus. The positively-charged C-Dots functionalized with PEI significantly affect cell cycle (by arresting the G0/G1 and G2/M phases) at a concentration of 100 μg mL^{-1} by entering into the cell nucleus.[117] However, the neutral C-Dots functionalized with polyethylene glycol do not affect cell morphology at concentrations up to 300 μg mL^{-1}, suggesting their higher biocompatibility. The hydrophobic thin films of C-Dots irradiated with blue light (470 nm) for 6 h is also found to be non-cytotoxic to the mouse fibroblast cell line NIH/3T3.[101] Yousaf *et al*. reported the capability of fluorine functionalized GQDs (FGQDs) for inhibition of the aggregation of human islet amyloid polypeptide (hIAPP) with a minimal cytotoxicity, highlighting the potential of FGQDs in the treatment of amyloidosis.[118] With a high charge density and the presence of hydrophobic groups, FGQDs can bind with the hIAPP monomer, prolong the aggregation time, and inhibit the conformational transition of hIAPP, thereby preventing the formation of mature fibrils. Red-fluorescent GQDs synthesized from *Mangifera indica* (mGQDs) with a size of 2–8 nm is reported to be biocompatible with the mouse fibroblast cell line L929 even at a high concentration of 0.1 mg mL^{-1}.[119]

Though the biocompatibility of carbon nanomaterials has been recognized, evaluation of the cytotoxicity is primarily conducted *in vitro* with only a handful of *in vivo* studies. Lacking the trial evidence, these cytotoxicity studies do not meet the evaluation criteria for clinical application of these nanomaterials. Table 2 summarizes several *in vivo* antibacterial trials of GO and C-Dots in animal models. Even in light of promising *in vivo* antibacterial properties for GO and C-Dots, studies on animal models have revealed potential accumulation of carbon nanomaterials, especially GO and rGO, in spleen, liver, and other internal organs. A comparison in cytotoxicity for GO, C-Dots, and selective metal (*e.g.*, Au, Ag), metal oxide (*e.g.*, TiO_2, ZnO), and metalloid (*e.g.*, Se, Te) nanoparticles is presented in Table 3. Although the cytotoxicity of GO and C-Dots are much lower than metal, metal oxide, and metalloid

Table 2 Summary of biomedical studies of GO and C-Dots in various animal models

Carbon nanomaterial (size)	Bacteria causing infection	Administration method	Antibacterial mechanism	*In vivo* effect	Ref.
GO (μm range)	*K. pneumoniae*	Intranasally into mouse lungs (respiratory infection)	ROS generation	Less tissue injury and prolonged survival of mice	49
GQDs (3–8 nm)	*S. aureus*	H_2O_2-GQD-Band-Aid for wound in mice	Peroxidase-like activity of GQD and production of $^{\bullet}OH$ radical	Better wound healing without erythema and edema, with the formation of scabs	98
Spd-CQDs (4.6 nm)	MRSA	Dressing material for MRSA infected wound in rat	Disruption of bacterial cell membrane	Better epithelial coverage, collagen secretion and accelerated wound healing	89
CQD_{Spds} (6 nm)	*S. aureus*	Topical ocular administration in rabbit for treatment of bacterial keratitis	Disruption of bacterial cell membrane	Induce opening of tight junctions of corneal epithelial cells leading to great antibacterial treatment of bacterial keratitis	90

Published on 05 Waysu 2018. Downloaded on 01/08/2024 7:53:25 AM.

nanoparticles, further studies are needed to understand potential medical complications associated with the accumulation of carbon nanomaterials, such as disruption of organ functions and development of chronic diseases. Additionally, an in-depth understanding of the pharmacokinetics of carbon nanomaterials will help in designing effective antibacterial carbon nanomaterials which can be easily excreted from human body.

5. Environmental toxicity

5.1 Graphene derivatives

The wide production and application of nanomaterials in recent years have generated major environmental impacts, such as increased human exposure to nanomaterials and nano-waste disposal.[120] The environmental impacts of graphene-based nanomaterials cannot be overlooked as they can affect the growth of vegetables, such as cabbage, tomatoes, spinach, lettuce, and plantain.[121,122] A study reveals that GO can accumulate in the root of wheat exposed to ^{13}C-GO, affecting the growth and development of the plant and disrupting the root structure.[123] This study also shows that GO at concentrations higher than 0.4 μg mL^{-1} can significantly inhibit the germination of wheat seeds. In contrast, another study shows that GO exposure in the concentration range of μg L^{-1} does not obviously influence germination, seed and root development, and flowering for *Arabidopsis thaliana*. Though GO can accumulate in root hair and parenchyma cells, translocation of GO into stem and leaf is not observed.[124] Interestingly, a recent work demonstrates that GO, when added to the soil in a mild dose at 50 μg mL^{-1}, enhances the germination of spinach and chive without any phytotoxic effect.[125] The abundant oxygen-containing functional groups in GO can assist water collection, and the hydrophobic sp^2 domains can mediate water transport to the seed to accelerate its germination.

The fate of graphene-based nanomaterials in the aquatic environment and porous media has been recently reviewed.[126] The environmental toxicity of nanomaterials highly depends on the nature of environment, such as salt water, fresh water, soil, and sediments. Also, organisms respond differently to the same nanomaterial under different environmental conditions.[127] The presence of GO in waste streams can impact bacterial viability, disrupt microbial species, and lower the levels of biochemical oxygen demand (BOD), nitrogen, phosphorus and other organics possibly *via* ROS generation, thus deteriorating the performance of biological wastewater treatment.[128] GO can pose toxic effects to algae, protozoans, freshwater cladoceran, white rot fungus, wild-nematodes, other aquatic organisms, some insects, and plant species in a dose-dependent manner.[123,129–139] For example, wild nematodes, upon a long-term exposure to thiolated GO at a concentration >100 μg L^{-1}, experience a high toxicity and severe accumulation of GO in both primary target organs, such as intestine, and secondary target organs, such as neurons and reproductive organs.[135] GO can cause oxidative stress and immune toxicity in zebra fish and also affect embryo development.[136,137,140] Studies on *Acheta domesticus* exposed to GO-containing food show multigenerational harmful effects, such as decreased reproductive ability and low cell vitality of the progeny.[139] In another study, GO at a concentration of 0.7 mg mL^{-1} can cause 90% mortality of brine shrimp larvae.[138]

The toxicity of GO in the aqueous environment depends on its residence time (as a fate factor) and the bioavailability (as an exposure factor).[141] In the presence of sunlight, GO sheets can be converted to rGO, increasing their toxicity to freshwater algae through increased shading effect, surface hydrophobicity, and membrane-damage ability.[130] The cytotoxic nature of GO can be mitigated significantly by surface functionalization of GO with biocompatible macromolecules.[142] The presence of humic acid in the aqueous environment can also mitigate the level of GO toxicity by changing GO morphology, structure, and surface negative charges, thus decreasing the interaction between GO and organism, and suppressing the GO-induced ROS.[143,144] However, Castro *et al*. reported contradicting observations for the effect of humic acid on the toxicity of GO toward different species in different medium.[127] For example, the presence of humic acid significantly decreases the toxicity of GO toward *Daphnia magna* and *Artemia salina*, however, humic acid increases the colloidal stability of GO in some culture media and increases the toxicity toward *Caenorhabditis elegans*. A report by Kurapati *et al*. reveals that human myeloperoxidase (hMPO), derived from human neutrophils, can degrade well dispersed GO in presence of a low concentration of H_2O_2 (200 μM) in aqueous media, but cannot degrade aggregated GO.[145] The observation encourages further development for biodegradation of GO in animal or human body.

5.2 C-Dots

The environmental toxicity of C-Dots is not well documented. C-Dots synthesized from β-alanine, a potential neuro-theranostics agent, can emit bright fluorescence and exhibit neuro-active properties, making them useful for visualization of key transport mechanisms and pathways in the nerve terminals.[146] However, it was also found that the presence of β-alanine-derived C-Dots at a high concentration in the air can pose potential risks of toxicity to the central nervous system in Wistar rats.[146] Like GO, GQDs can also affect embryonic development and increase mortality in zebra fish at concentrations above 50 μg mL^{-1}.[147] C-Dots derived from citric acid exhibit a dose-dependent and light-enhanced toxicity to yeast cells, *Pichia pastoris*.[148] Though C-Dots derived from citric acid and tris(hydroxymethyl)aminomethane can promote the fecundity of *Physa acuta* at low concentrations of 0.5 and 1.0 mg mL^{-1}, such fecundity is affected significantly with a chronic toxicity being observed at high concentrations of 3 mg mL^{-1} after a 12 day exposure.[149] Recently, Li *et al*. reported the degradability of less toxic C-Dots (with a particle size of 1.03–1.11 nm) derived from Vitamin C.[150] With strong antibacterial and antifungal activities at low concentrations (50–100 μg mL^{-1}), these biodegradable C-Dots are completely degraded into CO_2, CO, and H_2O under visible light in the air or a mild temperature of 37 °C after 20 days. The C-Dots in different growth media are easily degraded into CO_2 and CO, suggesting their potential *in vivo* degradability in living

 This journal is © The Royal Society of Chemistry 2019

Published on 05 Waysu 2018. Downloaded on 01/08/2024 7:53:25 AM.

Table 3 Comparison in cytotoxicity for GO, C-Dots, and selective metallic, metal oxide and metalloid nanoparticles

Material	Organism	Species/nature of cells	Size	Toxic concentration of nanomaterials	Organ/part affected	Mechanism of toxicity	Ref.
GO	Green algae	*Raphidocelis subcapitata*	110 nm (hydrodynamic size)	20 μg mL^{-1}	Growth inhibition	ROS generation and shading effect	129
	Marine algae	*Picochlorum* sp.	n/a	2.5 mg L^{-1}	Decrease concentration of chlorophyll *a* and affect growth rate	Shading effect	131
	Protozoan	*Euglena gracilis*	1–10 μm	2.5 mg L^{-1}	Inhibition of growth and the enhancement of malondialdehyde content and antioxidant enzyme activities	Shading effect and oxidative stress	132
	Freshwater cladoceran	*Ceriodaphnia dubia*	1 nm	1.25 mg L^{-1}	Reproduction inhibition and mortality	ROS generation	133
	White rot fungus	*Phanerochaete chrysosporium*	0.9 nm	4 mg mL^{-1}	Inhibition of weight gain, disorder of morphologies and loss of decomposition activity	Damage of cell wall by the sharp edges of GO	134
	Freshwater algae	*Chlorella pyrenoidosa*	2 nm	37.3 mg L^{-1}	Growth inhibition due to membrane damage	Shading effect, oxidative stress and physical penetration	130
	Waste water microbial community		n/a	50–300 mg L^{-1}	Reduction of bacterial metabolic activity, viability, and biological removal of nutrients	Accumulation of GO and ROS generation	128
	House cricket	*Acheta domesticus*	0.5–5 μm	20 and 200 μg g^{-1} of food	Reproductive dysfunction and lower cell vitality	Accumulation resulting in genetic material fragmentation	139
	Wild nematode	*Caenorhabditis elegans*	40–50 nm	>10 μg L^{-1}	Intestines, reproductive organs and neurons	Mutation of gas-1 due to accumulation and ROS generation	135
	Zebra fish		323.2 ± 23.7 nm (hydrodynamic size)	1 mg L^{-1}	Embryogenesis	Deposition of GO, alteration of chorionic proteins, oxidative stress and mitochondrial toxicity	143
	Zebra fish		<5 μm	10 mg mL^{-1}	Immunotoxicity with cellular alterations	Oxidative stress	136
	Wheat	Lunxuan 987	30 nm (hydrodynamic size)	≥0.4 mg mL^{-1}	Root	Oxidative stress induced by bioaccumulation	123
	Thale cress	*Arabidopsis thaliana*	40–60 nm	Range of μg L^{-1}	Growth inhibition	Shading effect	124
		HUVEC	0.4 and 0.8 μm	10 μg mL^{-1}	Cell toxicity without affecting cell morphology	ROS generation	106
		Human fibroblast cells	n/a	50 μg mL^{-1}	Cytotoxicity such as decreasing cell adhesion, inducing cell apoptosis, entering into lysosomes, mitochondrion, endoplasm, and cell nucleus	Accumulation of GO	110
	Mice		n/a	0.4 mg per mouse	Mice death and lung granuloma formation	GO conglomeration	110
		20S proteasome	0.5–3 μm	10 mg mL^{-1}	Suppression of proteolytic activity of proteasome	Adsorption of GO onto proteasome	111
C-Dots	Yeast cell	*Pichia pastoris*	3 nm	25 mg mL^{-1}	Cell shrinkage, hole formation on the surface of cells and growth inhibition	ROS generation	148
	Snail	*Physa acuta*	2.1–5.7 nm	3 mg mL^{-1}	Fecundity inhibition	Accumulation in visceral mass	149
	Zebra fish		2–5 nm	50 μg mL^{-1}	Embryonic malfunction and mortality	Accumulation of GQD	147
Ag NPs			2.338 nm	IC_{50} value 5.6 μg mL^{-1} 11.99 μg mL^{-1} 13.33 μg mL^{-1}	*In vitro* cytotoxicity against Ehrlich's ascites carcinoma (EAC), Jurkat and MCF-7 cells	Chromatin condensation, DNA fragmentation, cell cycle arrest at G2/M phase, up-regulation of Bax and caspase-3 and down-regulation of Bcl-2	156
Au NPs			15 nm	IC_{20} value 2.0 mM	Feline injection site sarcoma cell line	Decrease cellular proliferation	157

Published on 05 Waysu 2018. Downloaded on 01/08/2024 7:53:25 AM.

Table 3 (*continued*)

Material	Organism	Species/nature of cells	Size	Toxic concentration of nanomaterials	Organ/part affected	Mechanism of toxicity	Ref.
Pt NPs			20.12 nm	IC_{50} value 17.84 μg mL^{-1}	MCF-7 cell line	Reducing DNA synthesis and apoptosis-inducing cell cycle stages	158
TiO_2 NPs			Anatase 20–60 nm	50 μg mL^{-1}	Genotoxicity of peripheral blood mononuclear cells and lymphocytes	Oxidative DNA damage	159
			Rutile 30 × 100 nm	100 μg mL^{-1}			
			Mixture anatase/rutile 45–262 nm	100 μg mL^{-1}			
ZnO NPs		RAW 246.7 macrophage cells	∼37 nm	200 μg mL^{-1}	Cell death	Release of Zn^{2+} ions, ROS generation	160
Fe_2O_3 NPs	Zebra fish		5.7 nm	4.7–74.4 mg L^{-1}	Genotoxic effects and cell growth	Oxidative stress	161
Al_2O_3 NPs	Freshwater fish	*Oreochromis mossambicus*	40 nm	120–180 ppm	Histological anomalies	Accumulation of Al	162
CuO NPs	Mussels	*Mytilus galloprovincialis* and pulmonary TT1 cells	29.5 nm	5 mg L^{-1}	Hemocytes and gill cells	Dose-dependent ROS generation	163
CeO_2 NPs	Mussels	*Mytilus galloprovincialis*	26 ± 16 and 9± 4 nm	50 mg L^{-1}	Downregulation of immune systems	Loss of lysosomal membrane stability and a decrease in the phagocytosis capacity of the cells	164
SiO_2 NPs	Rats		20–30 nm	20 mg kg^{-1} body weight	Cognitive ability of rat	n/a	165
Se NPs	Rats		20 nm	0.05 mg kg^{-1} body weight	Overt toxicity	Accumulation of Se	166
Te NPs	Mice		40–200 nm	6 mg kg^{-1} body weight	Weight loss, renal and reproductive toxicity	Oxidative stress	167
Nanoscale fragments (Mixtures of elements)	Rice		68–187 nm	0.07–0.55 mg L^{-1}	Phytotoxicity (damage tochloroplasts and mitochondria)	Disorder of carbohydrate, amino acid and fatty acid metabolism	168

n/a: not available.

This journal is © The Royal Society of Chemistry 2019

Published on 05 Waysu 2018. Downloaded on 01/08/2024 7:53:25 AM.

organisms.[150] Therefore, further studies on the environmental impacts and degradability of nanomaterials should also focus on the interaction between nanomaterials and different organisms, mainly the aquatic biota, in addition to the long-term fate and behavior of distribution of these nanomaterials.

6. Conclusions

While GO and C-Dots are carbon nanomaterials with promising antimicrobial properties, major technological challenges limiting their effective design and practical application persist. For GO, the nanomaterial design strategies should be developed to eliminate undesired adsorption of biomolecules, protect basal plane from contamination, and increase the antibacterial activity without compromising its biocompatibility. Any structural defect in the carbon network will significantly affect the properties and effectiveness of the nanomaterial. Hence, one of the greatest challenges for large-scale production of graphene-based nanomaterials, such as GO, is to consistently maintain a high quality and uniform size for the synthesized nanomaterials with a low cost and high reproducibility for the synthesis process. Another technical difficulty is related to the colloidal stability of GO in dispersions. While GO can be easily dispersed in water and a wide number of solvents by mere sonication, the structural changes, folding, stacking of GO cannot be avoided upon a long term storage and repeated sonication. On the other hand, the facile synthesis and functionalization of C-Dots have enabled a precise control in charge density and functional group. This represents a great opportunity to address bacterial MDR issues by developing novel C-Dots with a selective antibacterial activity toward specific bacteria. Though reports are available for the synthesis of C-Dots in a gram scale, larger-scale synthesis remains a major challenge due to technical limitations similar to GO, such as synthesis reproducibility and consistent modulation of the properties of C-Dots, and cost effectiveness. As different types of carbon nanomaterials possess different properties based on the lateral size, surface charge, and surface functionalization, their cytotoxicity and biocompatibility for different cell lines should be extensively studied for safe biomedical applications. Additionally, acute and chronic cytotoxicity studies using animal models should be conducted for these carbon nanomaterials.

Conflicts of interest

There are no conflicts to declare.

Acknowledgements

This work was supported by the Ministry of Science and Technology of Taiwan under Contract No. 107-2113-M-019-004-MY3, 107-2622-M-019-001-CC2, and 107-2627-M-007-007-MY3 and supported by the Center of Excellence for the Oceans, National Taiwan Ocean University from The Featured Areas Research Center Program within the framework of the Higher Education Sprout Project by the Ministry of Education (MOE) in Taiwan.

References

1 World Health Organization, Antimicrobial Resistance: Global Report on Surveillance 2014, WHO.
2 https://www.cdc.gov/drugresistance/emerging.html, accessed April 2018.
3 S. I. Miller, *mBio.*, 2016, **7**, e01541–e01516.
4 S. Santajit and N. Indrawattana, *Biomed Res. Int.*, 2016, 2475067, DOI: 10.1155/2016/2475067.
5 T. S. Crofts, A. J. Gasparrini and G. Dantas, *Nat. Rev. Microbiol.*, 2017, **15**, 422–434.
6 S. B. Singh, K. Young and L. L. Silver, *Biochem. Pharmacol.*, 2017, **133**, 63–73.
7 S. U. Vetterli, K. Moehle and J. A. Robinson, *Bioorg. Med. Chem.*, 2016, **24**, 6332–6339.
8 L. Zimmermann, I. Das, J. Désiré, G. Sautrey, V. Barros, R. S. M. El Khoury, M.-P. Mingeot-Leclercq and J.-L. Décout, *J. Med. Chem.*, 2016, **59**, 9350–9369.
9 T. Chalopin, D. Alvarez Dorta, A. Sivignon, M. Caudan, T. I. Dumych, R. O. Bilyy, D. Deniaud, N. Barnich, J. Bouckaert and S. G. Gouin, *Org. Biomol. Chem.*, 2016, **14**, 3913–3925.
10 S. A. Jung, C. A. Chapman and W.-L. Ng, *PLoS Pathog.*, 2015, **11**, e1004837.
11 D. I. Andersson, D. Hughes and J. Z. Kubicek-Sutherland, *Drug Resist. Update.*, 2016, **26**, 43–57.
12 S. Garneau-Tsodikova and K. J. Labby, *Med. Chem. Commun.*, 2016, **7**, 11–27.
13 B. Pelaz, C. Alexiou, R. A. Alvarez-Puebla, F. Alves, A. M. Andrews, S. Ashraf, L. P. Balogh, L. Ballerini, A. Bestetti and C. Brendel, *et al.*, *ACS Nano*, 2017, **11**, 2313–2381.
14 G. Chen, I. Roy, C. Yang and P. N. Prasad, *Chem. Rev.*, 2016, **116**, 2826–2885.
15 M. Hoseinnejad, S. M. Jafari and I. Katouzian, *Crit. Rev. Microbiol.*, 2018, **44**, 161–181.
16 A. Raghunath and E. Perumal, *Int. J. Antimicrob. Agents*, 2017, **49**, 137–152.
17 D. Wang, Z. Lin, T. Wang, Z. Yao, M. Qin, S. Zheng and W. Lu, *J. Hazard. Mater.*, 2016, **308**, 328–334.
18 S. J. Soenen, W. J. Parak, J. Rejman and B. Manshian, *Chem. Rev.*, 2015, **115**, 2109–2135.
19 K. Zheng, M. I. Setyawati, D. T. Leong and J. Xie, *Chem. Mater.*, 2018, **30**, 2800–2808.
20 C. Cheng, S. Li, A. Thomas, N. A. Kotov and R. Haag, *Chem. Rev.*, 2017, **117**, 1826–1914.
21 P. Namdari, B. Negahdari and A. Eatemadi, *Biomed. Pharmacother.*, 2017, **87**, 209–222.
22 G. Reina, J. M. Gonzalez-Dominguez, A. Criado, E. Vazquez, A. Bianco and M. Prato, *Chem. Soc. Rev.*, 2017, **46**, 4400–4416.
23 H. Zhao, R. Ding, X. Zhao, Y. Li, L. Qu, H. Pei, L. Yildirimer, Z. Wu and W. Zhang, *Drug Discovery Today*, 2017, **22**, 1302–1317.
24 Z. Peng, X. Han, S. Li, A. O. Al-Youbi, A. S. Bashammakh, M. S. El-Shahawi and R. M. Leblanc, *Coord. Chem. Rev.*, 2017, **343**, 256–277.

Published on 05 Waysu 2018. Downloaded on 01/08/2024 7:53:25 AM.

25 Kenry, W. C. Lee, K. P. Loh and C. T. Lim, *Biomaterials*, 2018, **155**, 236–250.
26 X. Zou, L. Zhang, Z. Wang and Y. Luo, *J. Am. Chem. Soc.*, 2016, **138**, 2064–2077.
27 S. Szunerits and R. Boukherroub, *J. Mater. Chem. B*, 2016, **4**, 6892–6912.
28 H. E. Karahan, C. Wiraja, C. Xu, J. Wei, Y. Wang, L. Wang, F. Liu and Y. Chen, *Adv. Healthcare Mater.*, 2018, 1701406, DOI: 10.1002/adhm.201701406.
29 X. T. Zheng, A. Ananthanarayanan, K. Q. Luo and P. Chen, *Small*, 2015, **11**, 1620–1636.
30 I. P.-J. Lai, S. G. Harroun, S.-Y. Chen, B. Unnikrishnan, Y.-J. Li and C.-C. Huang, *Sens. Actuators, B*, 2016, **228**, 465–470.
31 C.-I. Weng, H.-T. Chang, C.-H. Lin, Y.-W. Shen, B. Unnikrishnan, Y.-J. Li and C.-C. Huang, *Biosens. Bioelectron.*, 2015, **68**, 1–6.
32 W. Bing, H. Sun, Z. Yan, J. Ren and X. Qu, *Small*, 2016, **12**, 4713–4718.
33 R. S. Santos, C. Figueiredo, N. F. Azevedo, K. Braeckmans and S. C. De Smedt, *Adv. Drug Delivery Rev.*, 2017, DOI: 10.1016/j.addr.2017.12.010.
34 S. N. Kale, R. Kitture, S. Ghosh, B. A. Chopade and J. V. Yakhmi, in *Antimicrobial Nanoarchitectonics*, ed. A. M. Grumezescu, Elsevier, 2017, ch. 11, pp. 279–321.
35 V. Palmieri, M. C. Lauriola, G. Ciasca, C. Conti, M. D. Spirito and M. Papi, *Nanotechnology*, 2017, **28**, 152001.
36 H. M. Hegab, A. ElMekawy, L. Zou, D. Mulcahy, C. P. Saint and M. Ginic-Markovic, *Carbon*, 2016, **105**, 362–376.
37 A. J. Huh and Y. J. Kwon, *J. Controlled Release*, 2011, **156**, 128–145.
38 N. Beyth, Y. Houri-Haddad, A. Domb, W. Khan and R. Hazan, *Evid.-Based Complementary Altern. Med.*, 2015, 246012.
39 K. Zheng, M. I. Setyawati, D. T. Leong and J. Xie, *Coord. Chem. Rev.*, 2018, **357**, 1–17.
40 A. Al-Jumaili, S. Alancherry, K. Bazaka and M. Jacob, *Materials*, 2017, **10**, 1066.
41 C. Liu, J. Guo, X. Yan, Y. Tang, A. Mazumder, S. Wu and Y. Liang, *Environ. Rev.*, 2017, **25**, 225–244.
42 S. Ye, K. Shao, Z. Li, N. Guo, Y. Zuo, Q. Li, Z. Lu, L. Chen, Q. He and H. Han, *ACS Appl. Mater. Interfaces*, 2015, **7**, 21571–21579.
43 M. Sametband, I. Kalt, A. Gedanken and R. Sarid, *ACS Appl. Mater. Interfaces*, 2014, **6**, 1228–1235.
44 X. Dong, M. M. Moyer, F. Yang, Y.-P. Sun and L. Yang, *Sci. Rep.*, 2017, **7**, 519.
45 F. M. P. Tonelli, V. A. M. Goulart, K. N. Gomes, M. S. Ladeira, A. K. Santos, E. Lorençon, L. O. Ladeira and R. R. Resende, *Nanomedicine*, 2015, **10**, 2423–2450.
46 G. Lalwani, M. D'Agati, A. M. Khan and B. Sitharaman, *Adv. Drug Delivery Rev.*, 2016, **105**, 109–144.
47 L. Hui, J.-G. Piao, J. Auletta, K. Hu, Y. Zhu, T. Meyer, H. Liu and L. Yang, *ACS Appl. Mater. Interfaces*, 2014, **6**, 13183–13190.
48 W. Hu, C. Peng, W. Luo, M. Lv, X. Li, D. Li, Q. Huang and C. Fan, *ACS Nano*, 2010, **4**, 4317–4323.
49 X. Wu, S. Tan, Y. Xing, Q. Pu, M. Wu and J. X. Zhao, *Colloids Surf., B*, 2017, **157**, 1–9.
50 S. Gurunathan, J. W. Han, A. A. Dayem, V. Eppakayala and J.-H. Kim, *Int. J. Nanomed.*, 2012, **7**, 5901–5914.
51 J. He, X. Zhu, Z. Qi, C. Wang, X. Mao, C. Zhu, Z. He, M. Li and Z. Tang, *ACS Appl. Mater. Interfaces*, 2015, **7**, 5605–5611.
52 S. Liu, M. Hu, T. H. Zeng, R. Wu, R. Jiang, J. Wei, L. Wang, J. Kong and Y. Chen, *Langmuir*, 2012, **28**, 12364–12372.
53 S. Liu, T. H. Zeng, M. Hofmann, E. Burcombe, J. Wei, R. Jiang, J. Kong and Y. Chen, *ACS Nano*, 2011, **5**, 6971–6980.
54 O. Akhavan and E. Ghaderi, *ACS Nano*, 2010, **4**, 5731–5736.
55 Y. Tu, M. Lv, P. Xiu, T. Huynh, M. Zhang, M. Castelli, Z. Liu, Q. Huang, C. Fan and H. Fang, *Nat. Nanotechnol.*, 2013, **8**, 594–601.
56 R. G. Combarros, S. Collado and M. Díaz, *J. Hazard. Mater.*, 2016, **310**, 246–252.
57 J. Chen, H. Peng, X. Wang, F. Shao, Z. Yuan and H. Han, *Nanoscale*, 2014, **6**, 1879–1889.
58 I. E. M. Carpio, C. M. Santos, X. Wei and D. F. Rodrigues, *Nanoscale*, 2012, **4**, 4746–4756.
59 Y. Chong, C. Ge, G. Fang, R. Wu, H. Zhang, Z. Chai, C. Chen and J.-J. Yin, *Environ. Sci. Technol. Lett.*, 2017, **51**, 10154–10161.
60 J. Wang, Y. Wei, X. Shi and H. Gao, *RSC Adv.*, 2013, **3**, 15776–15782.
61 F. Perreault, A. F. Faria, S. Nejati and M. Elimelech, *ACS Nano*, 2015, **9**, 7226–7236.
62 F. Zou, H. Zhou, D. Y. Jeong, J. Kwon, S. U. Eom, T. J. Park, S. W. Hong and J. Lee, *ACS Appl. Mater. Interfaces*, 2017, **9**, 1343–1351.
63 Z. Wang, D. Tonderys, S. E. Leggett, E. K. Williams, M. T. Kiani, R. S. Steinberg, Y. Qiu, I. Y. Wong and R. H. Hurt, *Carbon*, 2016, **97**, 14–24.
64 V. Palmieri, F. Bugli, M. C. Lauriola, M. Cacaci, R. Torelli, G. Ciasca, C. Conti, M. Sanguinetti, M. Papi and M. De Spirito, *ACS Biomater. Sci. Eng.*, 2017, **3**, 619–627.
65 M. A. Buccheri, D. D'Angelo, S. Scalese, S. F. Spanò, S. Filice, E. Fazio, G. Compagnini, M. Zimbone, M. V. Brundo, R. Pecoraro, A. Alba, F. Sinatra, G. Rappazzo and V. Privitera, *Nanotechnology*, 2016, **27**, 245704.
66 O. N. Ruiz, K. A. S. Fernando, B. Wang, N. A. Brown, P. G. Luo, N. D. McNamara, M. Vangsness, Y.-P. Sun and C. E. Bunker, *ACS Nano*, 2011, **5**, 8100–8107.
67 J. D. Mangadlao, C. M. Santos, M. J. L. Felipe, A. C. C. de Leon, D. F. Rodrigues and R. C. Advincula, *Chem. Commun.*, 2015, **51**, 2886–2889.
68 I. Barbolina, C. R. Woods, N. Lozano, K. Kostarelos, K. S. Novoselov and I. S. Roberts, *2D Mater.*, 2016, **3**, 025025.
69 M. D. Rojas-Andrade, G. Chata, D. Rouholiman, J. Liu, C. Saltikov and S. Chen, *Nanoscale*, 2017, **9**, 994–1006.
70 P. C. Henriques, I. Borges, A. M. Pinto, F. D. Magalhães and I. C. Gonçalves, *Carbon*, 2018, **132**, 709–732.
71 L. He, L. F. Dumée, C. Feng, L. Velleman, R. Reis, F. She, W. Gao and L. Kong, *Desalination*, 2015, **365**, 126–135.

 This journal is © The Royal Society of Chemistry 2019

Published on 05 Waysu 2018. Downloaded on 01/08/2024 7:53:25 AM.

72 M.-Y. Lim, Y.-S. Choi, J. Kim, K. Kim, H. Shin, J.-J. Kim, D. M. Shin and J.-C. Lee, *J. Membr. Sci.*, 2017, **521**, 1–9.
73 Y. L. F. Musico, C. M. Santos, M. L. P. Dalida and D. F. Rodrigues, *ACS Sustainable Chem. Eng.*, 2014, **2**, 1559–1565.
74 F. Perreault, M. E. Tousley and M. Elimelech, *Environ. Sci. Technol. Lett.*, 2014, **1**, 71–76.
75 X.-N. Yang, D.-D. Xue, J.-Y. Li, M. Liu, S.-R. Jia, L.-Q. Chu, F. Wahid, Y.-M. Zhang and C. Zhong, *Carbohydr. Polym.*, 2016, **136**, 1152–1160.
76 C. D. Grande, J. Mangadlao, J. Fan, A. D. Leon, J. Delgado-Ospina, J. G. Rojas, D. F. Rodrigues and R. Advincula, *Macromol. Symp.*, 2017, **374**, 1600114.
77 J. Zhu, J. Wang, J. Hou, Y. Zhang, J. Liu and B. Van der Bruggen, *J. Mater. Chem. A*, 2017, **5**, 6776–6793.
78 S. Ma, S. Zhan, Y. Jia and Q. Zhou, *ACS Appl. Mater. Interfaces*, 2015, **7**, 10576–10586.
79 J. Mohammadnejad, F. Yazdian, M. Omidi, A. D. Rostami, B. Rasekh and A. Fathinia, *Eng. Life Sci.*, 2018, **18**, 298–307.
80 J.-m. Peng, J.-c. Lin, Z.-y. Chen, M.-c. Wei, Y.-x. Fu, S.-s. Lu, D.-s. Yu and W. Zhao, *Mater. Sci. Eng., C*, 2017, **71**, 10–16.
81 M. S. Raghu, K. Y. Kumar, M. K. Prashanth, B. P. Prasanna, R. Vinuth and C. B. P. Kumar, *J. Water Process Eng.*, 2017, **17**, 22–31.
82 J. Li, X. Liu, J. Lu, Y. Wang, G. Li and F. Zhao, *J. Colloid Interface Sci.*, 2016, **484**, 107–115.
83 J. Zhang, B. Zhang, X. Chen, B. Mi, P. Wei, B. Fei and X. Mu, *Materials*, 2017, **10**, 239.
84 G. R. Navale, C. S. Rout, K. N. Gohil, M. S. Dharne, D. J. Late and S. S. Shinde, *RSC Adv.*, 2015, **5**, 74726–74733.
85 S. Ullah, A. Ahmad, F. Subhan, A. Jan, M. Raza, A. U. Khan, A.-U. Rahman, U. A. Khan, M. Tariq and Q. Yuan, *J. Photochem. Photobiol. B: Biology*, 2018, **183**, 342–348.
86 S. Panda, T. K. Rout, A. D. Prusty, P. M. Ajayan and S. Nayak, *Adv. Mater.*, 2018, **30**, 1702149.
87 Q. Dou, X. Fang, S. Jiang, P. L. Chee, T.-C. Lee and X. J. Loh, *RSC Adv.*, 2015, **5**, 46817–46822.
88 W.-S. Kuo, Y.-T. Shao, K.-S. Huang, T.-M. Chou and C.-H. Yang, *ACS Appl. Mater. Interfaces*, 2018, **10**, 14438–14446.
89 Y.-J. Li, S. G. Harroun, Y.-C. Su, C.-F. Huang, B. Unnikrishnan, H.-J. Lin, C.-H. Lin and C.-C. Huang, *Adv. Healthcare Mater.*, 2016, **5**, 2545–2554.
90 H.-J. Jian, R.-S. Wu, T.-Y. Lin, Y.-J. Li, H.-J. Lin, S. G. Harroun, J.-Y. Lai and C.-C. Huang, *ACS Nano*, 2017, **11**, 6703–6716.
91 S. G. Harroun, J.-Y. Lai, C.-C. Huang, S.-K. Tsai and H.-J. Lin, *ACS Infect. Dis.*, 2017, **3**, 777–779.
92 J. Yang, X. Zhang, Y.-H. Ma, G. Gao, X. Chen, H.-R. Jia, Y.-H. Li, Z. Chen and F. G. Wu, *ACS Appl. Mater. Interfaces*, 2016, **8**, 32170–32181.
93 A. Pramanik, S. Jones, F. Pedraza, A. Vangara, C. Sweet, M. S. Williams, V. Ruppa-Kasani, S. E. Risher, D. Sardar and P. C. Ray, *ACS Omega*, 2017, **2**, 554–562.
94 W.-S. Kuo, Y.-T. Shao, K.-S. Huang, T.-M. Chou and C.-H. Yang, *ACS Appl. Mater. Interfaces*, 2018, **10**, 14438–14446.
95 R. Jijie, A. Barras, J. Bouckaert, N. Dumitrascu, S. Szunerits and R. Boukherroub, *Colloids Surf., B*, 2018, **170**, 347–354.
96 L. Hui, J. Huang, G. Chen, Y. Zhu and L. Yang, *ACS Appl. Mater. Interfaces*, 2016, **8**, 20–25.
97 S. Su, C. B. Shelton and J. Qiu, Proceedings of the ASME 2013 International Mechanical Engineering Congress and Exposition, California, USA, Nov. 2013.
98 H. Sun, N. Gao, K. Dong, J. Ren and X. Qu, *ACS Nano*, 2014, **8**, 6202–6210.
99 M. J. Meziani, X. Dong, L. Zhu, L. P. Jones, G. E. LeCroy, F. Yang, S. Wang, P. Wang, Y. Zhao, L. Yang, R. A. Tripp and Y.-P. Sun, *ACS Appl. Mater. Interfaces*, 2016, **8**, 10761–10766.
100 B. Z. Ristic, M. M. Milenkovic, I. R. Dakic, B. M. Todorovic-Markovic, M. S. Milosavljevic, M. D. Budimir, V. G. Paunovic, M. D. Dramicanin, Z. M. Markovic and V. S. Trajkovic, *Biomaterials*, 2014, **35**, 4428–4435.
101 N. K. Stanković, M. Bodik, P. Šiffalovič, M. Kotlar, M. Mičušik, Z. Špitalsky, M. Danko, D. D. Milivojević, A. Kleinova, P. Kubat, Z. Capakova, P. Humpoličeк, M. Lehocky, B. M. Todorović Marković and Z. M. Marković, *ACS Sustainable Chem. Eng.*, 2018, **6**, 4154–4163.
102 W.-S. Kuo, C.-Y. Chang, H.-H. Chen, C.-L. L. Hsu, J.-Y. Wang, H.-F. Kao, L. C.-S. Chou, Y.-C. Chen, S.-J. Chen, W.-T. Chang, S.-W. Tseng, P.-C. Wu and Y.-C. Pu, *ACS Appl. Mater. Interfaces*, 2016, **8**, 30467–30474.
103 M. M. Al Awak, P. Wang, S. Wang, Y. Tang, Y.-P. Sun and L. Yang, *RSC Adv.*, 2017, **7**, 30177–30184.
104 M. Ema, M. Gamo and K. Honda, *Regul. Toxicol. Pharmacol.*, 2017, **85**, 7–24.
105 Y. Volkov, J. McIntyre and A. Prina-Mello, *2D Mater.*, 2017, **4**, 022001.
106 S. Das, S. Singh, V. Singh, D. Joung, J. M. Dowding, D. Reid, J. Anderson, L. Zhai, S. I. Khondaker, W. T. Self and S. Seal, *Part. Part. Syst. Charact.*, 2013, **30**, 148–157.
107 Y. Chong, C. Ge, Z. Yang, J. A. Garate, Z. Gu, J. K. Weber, J. Liu and R. Zhou, *ACS Nano*, 2015, **9**, 5713–5724.
108 G. Duan, S.-G. Kang, X. Tian, J. A. Garate, L. Zhao, C. Ge and R. Zhou, *Nanoscale*, 2015, **7**, 15214–15224.
109 J.-H. Liu, S.-T. Yang, H. Wang, Y. Chang, A. Cao and Y. Liu, *Nanomedicine*, 2012, **7**, 1801–1812.
110 K. Wang, J. Ruan, H. Song, J. Zhang, Y. Wo, S. Guo and D. Cui, *Nanoscale Res. Lett.*, 2011, **6**, 8.
111 X. Ma, S. Lee, X. Fei, G. Fang, T. Huynh, Y. Chong, Z. Chai, C. Ge and R. Zhou, *Nanotoxicology*, 2018, **12**, 185–200.
112 K.-P. Wen, Y.-C. Chen, C.-H. Chuang, H.-Y. Chang, C.-Y. Lee and N.-H. Tai, *J. Appl. Toxicol.*, 2015, **35**, 1211–1218.
113 D. A. Jasim, H. Boutin, M. Fairclough, C. Ménard-Moyon, C. Prenant, A. Bianco and K. Kostarelos, *Appl. Mater. Today*, 2016, **4**, 24–30.
114 N. K. Nirmal, K. K. Awasthi and P. J. John, *Basic Clin. Pharmacol Toxicol.*, 2017, **121**, 202–210.
115 A. Skovmand, A. Jacobsen Lauvås, P. Christensen, U. Vogel, K. Sørig Hougaard and S. Goericke-Pesch, *Part. Fibre Toxicol.*, 2018, **15**, 10.

Published on 05 Waysu 2018. Downloaded on 01/08/2024 7:53:25 AM.

116 J. Bi, Y. Li, H. Wang, Y. Song, S. Cong, D. Li, D. Zhou, B.-W. Zhu and M. Tan, *New J. Chem.*, 2017, **41**, 8490–8496.
117 M. Havrdova, K. Hola, J. Skopalik, K. Tomankova, M. Petr, K. Cepe, K. Polakova, J. Tucek, A. B. Bourlinos and R. Zboril, *Carbon*, 2016, **99**, 238–248.
118 M. Yousaf, H. Huang, P. Li, C. Wang and Y. Yang, *ACS Chem. Neurosci.*, 2017, **8**, 1368–1377.
119 M. K. Kumawat, M. Thakur, R. B. Gurung and R. Srivastava, *ACS Sustainable Chem. Eng.*, 2017, **5**, 1382–1391.
120 J. R. Lead, G. E. Batley, P. J. J. Alvarez, M.-N. Croteau, R. D. Handy, M. J. McLaughlin, J. D. Judy and K. Schirmer, *Environ. Toxicol. Chem.*, 2018, **37**, 2029–2063.
121 P. Begum, R. Ikhtiari and B. Fugetsu, *Carbon*, 2011, **49**, 3907–3919.
122 M. Ghorbanpour, A. H. K. Farahani and J. Hadian, *Ecotoxicol. Environ. Saf.*, 2018, **148**, 910–922.
123 L. Chen, C. Wang, H. Li, X. Qu, S.-T. Yang and X.-L. Chang, *Environ. Sci. Technol.*, 2017, **51**, 10146–10153.
124 S. Zhao, Q. Wang, Y. Zhao, Q. Rui and D. Wang, *Environ. Toxicol. Pharmacol.*, 2015, **39**, 145–156.
125 Y. He, R. Hu, Y. Zhong, X. Zhao, Q. Chen and H. Zhu, *Nano Res.*, 2018, **11**, 1928–1937.
126 X. Ren, J. Li, C. Chen, Y. Gao, D. Chen, M. Su, A. Alsaedi and T. Hayat, *Environ. Sci.: Nano*, 2018, **5**, 1298–1340.
127 V. L. Castro, Z. Clemente, C. Jonsson, M. Silva, J. H. Vallim, A. M. Z. de Medeiros and D. S. T. Martinez, *Environ. Toxicol. Chem.*, 2018, **37**, 1998–2012.
128 F. Ahmed and D. F. Rodrigues, *J. Hazard. Mater.*, 2013, **256–257**, 33–39.
129 P. F. M. Nogueira, D. Nakabayashi and V. Zucolotto, *Aquat. Toxicol.*, 2015, **166**, 29–35.
130 J. Zhao, X. Cao, Z. Wang, Y. Dai and B. Xing, *Water Res.*, 2017, **111**, 18–27.
131 L. J. Hazeem, M. Bououdina, E. Dewailly, C. Slomianny, A. Barras, Y. Coffinier, S. Szunerits and R. Boukherroub, *Environ. Sci. Pollut. Res.*, 2017, **24**, 4144–4152.
132 C. Hu, Q. Wang, H. Zhao, L. Wang, S. Guo and X. Li, *Chemosphere*, 2015, **128**, 184–190.
133 J. P. Souza, F. P. Venturini, F. Santos and V. Zucolotto, *Chemosphere*, 2018, **190**, 218–224.
134 J. Xie, Z. Ming, H. Li, H. Yang, B. Yu, R. Wu, X. Liu, Y. Bai and S.-T. Yang, *Chemosphere*, 2016, **151**, 324–331.
135 X. Ding, J. Wang, Q. Rui and D. Wang, *Sci. Total Environ.*, 2018, **616-617**, 29–37.
136 M. Chen, J. Yin, Y. Liang, S. Yuan, F. Wang, M. Song and H. Wang, *Aquat. Toxicol.*, 2016, **174**, 54–60.
137 Z. Clemente, V. L. S. S. Castro, L. S. Franqui, C. A. Silva and D. S. T. Martinez, *Environ. Pollut.*, 2017, **225**, 118–128.
138 T. Mesarič, C. Gambardella, T. Milivojević, M. Faimali, D. Drobne, C. Falugi, D. Makovec, A. Jemec and K. Sepčić, *Aquat. Toxicol.*, 2015, **163**, 121–129.
139 M. Dziewięcka, P. Witas, J. Karpeta-Kaczmarek, J. Kwaśniewska, B. Flasz, K. Balin and M. Augustyniak, *Sci. Total Environ.*, 2018, **635**, 947–955.
140 W. Zou, Q. Zhou, X. Zhang, L. Mu and X. Hu, *Ecotoxicol. Environ. Saf.*, 2018, **159**, 221–231.
141 Y. Deng, J. Li, M. Qiu, F. Yang, J. Zhang and C. Yuan, *Int. J. Life Cycle Ass.*, 2017, **22**, 222–236.
142 Y. Li, L. Feng, X. Shi, X. Wang, Y. Yang, K. Yang, T. Liu, G. Yang and Z. Liu, *Small*, 2014, **10**, 1544–1554.
143 Y. Chen, C. Ren, S. Ouyang, X. Hu and Q. Zhou, *Environ. Sci. Technol.*, 2015, **49**, 10147–10154.
144 Y. Zhang, T. Meng, X. Guo, R. Yang, X. Si and J. Zhou, *Chemosphere*, 2018, **197**, 749–758.
145 R. Kurapati, J. Russier, M. A. Squillaci, E. Treossi, C. Ménard-Moyon, A. E. Del Rio-Castillo, E. Vazquez, P. Samorì, V. Palermo and A. Bianco, *Small*, 2015, **11**, 3985–3994.
146 T. Borisova, M. Dekaliuk, N. Pozdnyakova, A. Pastukhov, M. Dudarenko, M. Galkin, M. Malysheva, A. Borysov, S. G. Vari and A. P. Demchenko, *Advanced Materials: TechConnect Briefs*, 2017, **1**, 337–340.
147 Z. G. Wang, R. Zhou, D. Jiang, J. E. Song, Q. Xu, J. Si, Y. P. Chen, X. Zhou, L. Gan, J. Z. Li, H. Zhang and B. Liu, *Biomed. Environ. Sci.*, 2015, **28**, 341–351.
148 Z. Bagheri, H. Ehtesabi, Z. Hallaji, H. Latifi and E. Behroodi, *Ecotoxicol. Environ. Saf.*, 2018, **161**, 245–250.
149 X. Sun, X. Jin, W. Pan, E. Guo, W. Liu, D. Li, K. Lu, S. Si, N. Zhang, Z. Jia, Y. Shi, Q. Li and J. Wang, *J. Nanosci. Nanotechnol.*, 2016, **16**, 648–653.
150 H. Li, J. Huang, Y. Song, M. Zhang, H. Wang, F. Lu, H. Huang, Y. Liu, X. Dai, Z. Gu, Z. Yang, R. Zhou and Z. Kang, *ACS Appl. Mater. Interfaces*, 2018, **10**, 26936–26946.
151 S. Agnihotri, S. Mukherji and S. Mukherji, *RSC Adv.*, 2014, **4**, 3974–3983.
152 M. M. Mohamed, S. A. Fouad, H. A. Elshoky, G. M. Mohammed and T. A. Salaheldin, *Int. J. Vet. Sci. Med.*, 2017, **5**, 23–29.
153 T. K. Jana, A. Pal, A. K. Mandal, S. Sarwar, P. Chakrabarti and K. Chatterjee, *ChemistrySelect*, 2017, **2**, 3068–3077.
154 V. L. Prasanna and R. Vijayaraghavan, *Langmuir*, 2015, **31**, 9155–9162.
155 I. Chauhan and P. Mohanty, *Cellulose*, 2015, **22**, 507–519.
156 P. Maity, M. Bepari, A. Pradhan, R. Baral, S. Roy and S. Maiti Choudhury, *Colloids Surf., B*, 2018, **161**, 111–120.
157 J. Z. Benton, R. J. Williams, A. Patel, K. Meichner, J. Tarigo, K. Nagata, T. D. Pethel and R. M. Gogal, *Res. Vet. Sci.*, 2018, **117**, 104–110.
158 B. Şahin, A. Aygün, H. Gündüz, K. Şahin, E. Demir, S. Akocak and F. Şen, *Colloids Surf., B*, 2018, **163**, 119–124.
159 C. Andreoli, G. Leter, B. De Berardis, P. Degan, I. De Angelis, F. Pacchierotti, R. Crebelli, F. Barone and A. Zijno, *J. Appl. Toxicol.*, 2018, 1–12.
160 B. Wang, Y. Zhang, Z. Mao, D. Yu and C. Gao, *J. Nanosci. Nanotechnol.*, 2014, **14**, 5688–5696.
161 R. A. R. Villacis, J. S. Filho, B. Piña, R. B. Azevedo, A. Pic-Taylor, J. F. Mazzeu and C. K. Grisolia, *Aquat. Toxicol.*, 2017, **191**, 219–225.
162 M. Murali, P. Athif, P. Suganthi, A. S. Bukhari, H. E. S. Mohamed, H. Basu and R. K. Singhal, *Environ. Toxicol. Pharmacol.*, 2018, **59**, 74–81.

 This journal is © The Royal Society of Chemistry 2019

163 A. Katsumiti, A. J. Thorley, I. Arostegui, P. Reip, E. Valsami-Jones, T. D. Tetley and M. P. Cajaraville, *Toxicol. In Vitro*, 2018, **48**, 146–158.
164 M. Sendra, M. Volland, T. Balbi, R. Fabbri, M. P. Yeste, J. M. Gatica, L. Canesi and J. Blasco, *Aquat. Toxicol.*, 2018, **200**, 13–20.
165 A. Salem, A. Oudhabechi and M. Sakly, *Arch. Environ. Occup. Health*, 2018, 1–19.
166 N. Hadrup, K. Loeschner, K. Mandrup, G. Ravn-Haren, H. L. Frandsen, E. H. Larsen, H. R. Lam and A. Mortensen, *Drug Chem. Toxicol.*, 2018, 1–8.
167 S. Najimi, M. Shakibaie, E. Jafari, A. Ameri, N. Rahimi, H. Forootanfar, M. Yazdanpanah and H. R. Rahimi, *Regul. Toxicol. Pharmacol.*, 2017, **90**, 222–230.
168 X. Hu, C. Ren, W. Kang, L. Mu, X. Liu, X. Li, T. Wang and Q. Zhou, *Sci. Total Environ.*, 2018, **626**, 1332–1341.

Published on 05 Waysu 2018. Downloaded on 01/08/2024 7:53:25 AM.